Metabolic impact of trans 10, cis 12-conjugated linoleic acid in pai transgenic mice

Yu Rao [1,2,3,#], Shi-Li Li [4,#], Mei-Juan Li [5,#], Bao-Zhu Wang [1,#], Yang-Yang Wang [1], Lu-Wen Liang [1], Shuai Yu [1], Zong-Ping Liu [1], Sheng Cui [3], Ke-Mian Gou [1,2,3,*]

[1] *Institute of Comparative Medicine,* [2] *Jiangsu Co-innovation Center for Prevention and Control of Important Animal Infectious Diseases and Zoonoses,* [3] *Institute of Reproduction and Metabolism, College of Veterinary Medicine, Yangzhou University, Yangzhou 225009, China*;

[4] *Department of Internal Medicine, the University of Texas Southwestern Medical Center, Dallas, Texas 75390, USA*;

[5] *Institute of Animal Husbandry and Veterinary Science, Guizhou Academy of Agricultural Sciences, Guiyang 550005, China*.

[#] YR, SLL, MJL, and BZW contributed equally to this work.

* Corresponding author: Ke-Mian Gou, College of Veterinary Medicine, Yangzhou University, Yangzhou 225009, China. **Email**: gou@yzu.edu.cn

Declarations of interest: none

Abbreviations: CLA, conjugated linoleic acid; LA, linoleic acid; t10c12, *trans* 10, *cis* 12; pai, *Propionibacterium acnes* isomerase; wt, wild-type; FGF21, fibroblast growth factor 21; UCP, uncoupling protein; AMPK, AMP-activated protein kinase; BAT, brown adipose tissue; WAT, white adipose tissue; FAs, fatty acids

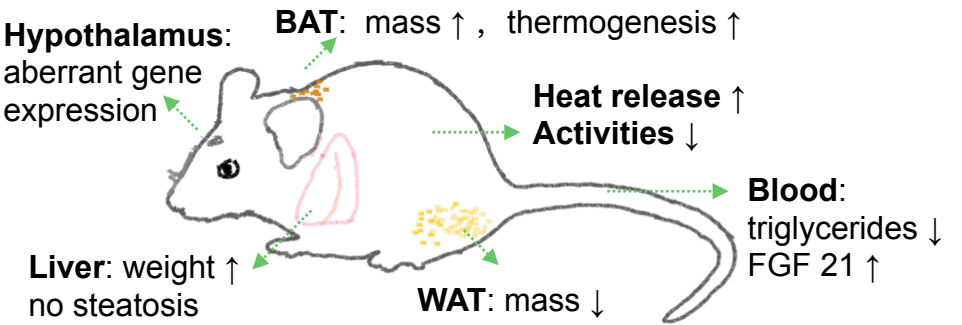

PAI transgenic mice
(producing trans 10, cis 12-CLA)

Graphical Abstract

1. A transgenic mouse itself can produce trans 10, cis 12-conjugated linoleic acid.
2. Mice showed more heat release and few activities.
3. Conjugated linoleic acid induces excess FGF21 and reduced triglycerides in the blood.
4. Conjugated linoleic acid promotes the mass and thermogenesis of brown adipose tissues.
5. Conjugated linoleic acid results in aberrant gene expression in the hypothalamus.

Highlight

Abstract

Introduction: Trans 10, *cis* 12-conjugated linoleic acid (t10c12-CLA) from ruminant-derived foodstuffs can induce body fat loss in mammals after oral administration, while its mechanism on fat reduction has yet to be clarified fully until now.

Methods: In the current study, a transgenic mouse that produces t10c12-CLA has been generated via the insertion of the Propionibacterium acnes isomerase (Pai) expression cassette into the Rosa26 locus, and its male offspring were used to decipher an irreversible long-term impact of t10c12-CLA on health and its mechanism of action.

Results: Compared to their wild-type C57BL/6J littermates, comprehensive phenotype profiling of biallelic pai/pai mice indicated that white fat was decreased while brown fat was increased reversely; meanwhile, more heat was released and the central activities were reduced. Besides decreased plasma triglycerides in both pai genotypes and increased serum FGF21 in pai/wt mice, RNA and protein analysis revealed that the thermogenesis capacity of brown adipose tissues was increased via pAMPK and UCP2 over-expression.

Conclusion: The results indicate that the t10c12-CLA-induced fat loss might be caused by the excess FGF21 and the increased mass and extra thermogenesis of brown adipose tissue in transgenic mice.

Keywords: conjugated linoleic acid; adipose tissue; obesity; thermogenesis; FGF21; hypothalamus

21 # 1. Introduction

22 *Trans* 10, *cis* 12-conjugated linoleic acid (t10c12-CLA), one of the isomers of linoleic
23 acid (18:2n-6, LA), is naturally present in ruminant-derived foodstuffs. It is estimated that a
24 person can take about 9~20 mg of t10c12-CLA from foodstuffs daily [1]. Since the effect of
25 t10c12-CLA on body fat loss in mice [2] and milk fat depression in cows [3] was reported,
26 numerous studies tried to explore its mechanism on lipid metabolism. Some studies revealed
27 that t10c12-CLA induces fat reduction by reducing food intake, modulating lipid metabolism,
28 increasing energy expenditure, and/or browning WAT [4-6]. Still, some of these reports
29 showed contradictory results sometimes. That is, the mechanism of action of t10c12-CLA on
30 fat reduction has yet to be clarified fully until now.

31 Meanwhile, other studies also indicated that t10c12-CLA influenced the metabolism or
32 physiological roles of some critical fatty acids (FAs), such as palmitic, stearic, oleic, linoleic,
33 arachidonic, docosahexaenoic acids and/or their derived leukotrienes signals/hormonal
34 molecules via affecting their contents in various tissues [7-10] based on the level of dietary fat
35 and the degree of host obesity [9, 11]. Furthermore, these studies in mice fed with a t10c12-
36 CLA diet revealed approximately 0.1-1.5% of t10c12-CLA in the brain and eye [12], milk [8],
37 adipose tissues [7], liver [7, 9], heart, spleen, kidney, muscle, and serum [9], suggesting that
38 t10c12-CLA might have a systemic impact on the body. Actually, besides anti-obesity, a few
39 studies also showed the connections between t10c12-CLA and hepatic steatosis [5, 13], pro-
40 inflammatory effects [13], and even intestinal microbiota in mice [14], suggesting the potential
41 risk of use of t10c12-CLA.

42 For naturally t10c12-CLA present at very low concentrations, most t10c12-CLA studies
43 or applications used a chemically CLA mixture prepared by industrial isomerisation. CLA

44 mixture usually contains approximately equal amounts of t10c12-CLA and *cis* 9, *trans* 11-CLA
45 (c9t11-CLA), typically 80–95% of total CLA, and other minor isomers, such as *trans*, *trans*
46 isomers [6]. To reveal the whole and exact t10c12-CLA's impact that might be offset or masked
47 by c9t11-CLA [6] or trans fatty acids [15] in the CLA mixtures, we seek the possibility of
48 producing t10c12-CLA by an animal itself so we might investigate it's long-term impact and
49 mechanism of action in a novel way.

50 Based on the reports that *Propionibacterium acnes* isomerase (PAI) can successfully
51 convert LA into t10c12-CLA in recombinant lactic acid bacteria [7, 9] and transgenic plants
52 [16], We produced t10c12-CLA efficiently in murine 3T3 cells [17]. Then we established a
53 pai-transgenic mouse previously [18]; unfortunately, the pai-expressing cassette was randomly
54 integrated into the Myh11 gene in this mouse, resulting in the death of homozygous mice after
55 birth due to gastric inflation and bladder without urinating ability [19].

56 In the present study, we produced a novel transgenic founder in which the pai-expressing
57 cassette was knocked into the Rosa26 locus by the CRISPR-Cas9 technique. The results
58 indicated that the pai/pai mice reduced white fat and lowered triglycerides (TGs) in the blood
59 but had no changes in hormones involved in energy intake, stress response, inflammation, and
60 fatty liver, suggesting long-term exposure to t10c12-CLA is safe, at least in male mammals.
61 Furthermore, we first revealed that increased FGF21 in the blood and more heat released by
62 brown fat resulted in white fat reduction in pai mice. The results shed light on the mechanism
63 of action of t10c12-CLA. Moreover, aberrant expression of the hypothalamic genes suggests
64 that t10c12-CLA could have other potential impacts on health. Thus, the use of t10c12-CLA
65 in anti-obesity practice or clinic trials should be closely monitored to ensure proper and safe
66 application.

67 ## 2. Materials and Methods

68 ### 2.1. Chemicals

69 Unless otherwise stated, all chemicals were purchased from Sigma (USA) or Sinopharm
70 Chemical Reagent Co., Ltd. (Shanghai, China). Restriction endonucleases were purchased
71 from New England Biolabs Inc (USA).

72 ### 2.2. Vector construction

73 The pRosa-pai vector was constructed as follows. In brief, based on the nucleotide
74 sequence of the Pai gene of *Propionibacterium acnes* (GenBank accession number
75 AX062088), the codon-optimized Pai gene was synthesised, which added the 6 x His affinity
76 tag sequence immediately upstream of the terminal codon. It has been confirmed that gene
77 transfection with this vector in murine 3T3 cells led to t10c12-CLA production [17]. On this
78 basis, the Pai expression vector was firstly generated after insertion into the *Eco*R I site of the
79 pCAGGS vector (Gift from Dr Timothy J. Ley, The Washington University, St. Louis), in
80 which the Pai gene was under the control of the cytomegalovirus enhancer and the chicken
81 beta-actin promoter (CAG promoter). After two molecular cloning steps of enzymic
82 modification, the CAG-pai expression cassette was inserted into the Pac I and Asc I sites of the
83 pROSA26-PA backbone vector (Gift from Dr Frank Costantini, Addgene plasmid#21271;
84 http://n2t.net/addgene:21271) to generate the pRosa-pai vector.

85 The pRosa-Cas9 vector was constructed as follows. Briefly, the CAG promoter sequence
86 of Cas9 in pDG330 plasmid (Gift from Dr Paul Thomas; Addgene plasmid # 100898;
87 http://n2t.net/addgene:100898) was replaced by the EF-1α promoter from the plasmid
88 pEF.myc.ER-E2-Crimson (Gift from Dr Benjamin Glick; Addgene plasmid # 38770;

89 http://n2t.net/addgene:38770) followed by insertion of the sgRNAs sequences (5-
90 actccagtctttctagaaga-3, from reference [20]) into Bbs I sites to generate the pRosa-Cas9 vector
91 which included the Cas9 gene driven by EF-1α promoter and dual gRNA expression cassettes.

92 **2.3. Pronuclear microinjection**

93 Purified pRosa-Cas9 plasmid DNA at a final concentration of 10 ng/μl and the fragments
94 of pRosa-pai plasmid after digestion by Pvu I + Sal I enzymes at a final concentration of
95 50~100 ng/μl were mixed well and used for pronuclear co-microinjection immediately.

96 **2.4. Mice**

97 Mice were obtained from the Laboratory Animal Centre, Yangzhou University, China.
98 All animal experiments were performed following the Committee for Experimental Animals
99 of Yangzhou University. Mice were maintained in a light-controlled room (12L:12D, lights on
100 at 0700 h) at a temperature of 22-23°C and were fed ad libitum with a standard diet containing
101 10% kcal% fat.

102 Embryos from superovulated D6B2F1 females mated with C57BL/6J male mice were
103 used to produce the transgenic mice. The transgenic founders were backcrossed to C57BL/6J
104 mice more than eight generations before analysis in the current study. The biallelic (pai/pai),
105 monoallelic (pai/wt), and wild-type (wt) male offsprings from the pai/wt matings were used in
106 this study.

107 **2.5. Diets**

108 New diets containing 10% kcal% fat were prepared per month under sterile conditions
109 according to formula No. D12450H of OpenSource DIETS^{TM} (Research Diets Inc., NJ, USA).
110 The formula D12450H and the sources of the food-grade ingredients for the diets are listed in

111 Supplementary Table 1. Fatty acid compositions in diets were spot-checked by gas
112 chromatography to examine the contents of linoleic acid and t10c12-CLA. One kilogram of
113 diet contained approximately 20 g of LA, and no t10c12-CLA was detected in diet samples.

114 **2.6. Transgene characterisation**

115 Genomic DNA from the tail tissues was used for nucleic acid analysis. The presence of
116 the pai transgene was assayed to amplify the 514-bp pai fragments (All primer sequences and
117 annealing temperatures were listed in Supplementary Table 2). The same insertion site was
118 assayed to amplify the 605-bp fragments that spanned the insertional Rosa26 area. The PCR
119 amplification was performed as follows: 30 cycles at 94°C for 30 sec, 57°C for 30 sec, and
120 72°C for 40 sec.

121 Southern blot was performed according to the standard procedure. In brief, 10 μg of
122 genomic DNA was first digested with the EcoR I enzyme for 12-16 h at 37°C and subjected to
123 1% agarose gel electrophoresis, then transferred onto the Hybond-N^+ membrane (Amersham,
124 UK). The membrane was subsequently hybridised with the DIG (Roche, Germany) labelled
125 probes according to the manufacturer's protocol, using alkaline phosphatase labelled anti-Dig
126 antibody (Roche) and CDP-STAR solution to develop the photos.

127 **2.7. Western blot**

128 Western blot was performed according to the standard procedures. Briefly, total protein
129 extracts from 20 mg tissues were quantified, and 20 μg protein extracts were separated with
130 10-15% SDS-PAGE gel and transferred to the PVDF membranes (Millipore ISEQ00010,
131 Merck). Membranes were blocked and hybridised with the respective primary antibody alone
132 or mixed with the anti-beta-actin antibody (Proteintech Group, Inc, China, 20536-1-AP)
133 followed by HPR-labelled goat anti-rabbit IgG (Santa Cruz Biotechnology, sc-2004). The

134 image was developed using the SuperSignal™ West Femto substrate (ThermoFisher, USA).
135 After subtracting the local background, the bands were quantified using Image software (Media
136 Cybernetics, USA). The primary antibodies included rabbit antibodies to His-tag (Proteintech
137 Group, 10001-0-AP), CPT1B (Proteintech, 22170-1-AP), UCP2 (Proteintech, 11081-1-AP),
138 FGF21 (Abcam Inc, USA, ab171941), pAMPK (Thr183 + Thr172, Abcam, AB133448),
139 AMPK (Abcam, ab207442), FASN (Abcam, AB128870), UCP1 (Abcam, ab234430), GRP78
140 BiP (Abcam, ab108613), PPAR-Γ (Wanleibio Ltd, China, WL01800), PGC1A (Wanleibio,
141 WL02123), and Phospho-HSL (Ser563, Cell Signaling Technology, #4139).

142 **2.8. RNA analysis**

143 Total RNA was extracted from tissues using the RNAiso Plus kit and treated with DNase
144 I (TaKaRa, China). The purified RNA was used for first-strand cDNA synthesis, and reverse
145 transcription was performed using an M-MLV reverse transcriptase with oligo-dT primers
146 according to the manufacturer's instructions (Promega, USA). For RT-PCR, the resulting
147 cDNA was used for PCR amplification with the Pai-specific primers (Supplementary Table 2)
148 that produced a 164-bp fragment. A 78-bp fragment of the Gapdh gene was amplified under
149 the same conditions and used as an endogenous control. PCR amplification was performed as
150 follows: 30 cycles of 94°C for 30 sec, 60°C for 30 sec, and 72°C for 30 sec.

151 All real-time PCRs were carried out in 96-well plates using ChamQ SYBR qPCR Master
152 Mix kit in the ABI Prism 7500 Sequence Detection System (Applied Biosystems, USA) at
153 95°C, 2 min, one cycle; 95°C, 5 sec, 60°C, 32 sec, 40 cycles. Three replicates were included
154 for each sample. The relative transcriptional level of a target gene was normalised to the one
155 of endogenous gene expression of Gapdh, ApoB, or 36B4 using the method of $2^{-\Delta\Delta Ct}$. All genes'
156 full names and these primer sequences are listed in Supplementary Table 3.

157 **2.9. RNA sequencing**

158 The RNA-seq was used to identify whole transcriptome differences in the BAT from wt
159 (n=2) and pai/pai (n=3) mice at 12 weeks. Total RNAs were analysed by BGI Genomics
160 company (China) using the DNBSEQ platform. Clean reads were aligned to *Mus musculus*
161 genome GCF_000001635.26_GRCm38.p6, and the expression level was normalised as FPKM
162 with gene annotation file. Differential expressional genes and functional enrichment for KEGG
163 had plotted an online platform for data analysis and visualisation
164 (http://www.bioinformatics.com.cn).

165 **2.10. Gas chromatography**

166 According to the modified method described by Jenkins [21], the procedure of two-step
167 trans-esterification that utilised sodium methoxide followed by shorter methanolic HCl was
168 used to methylate each organ/tissue homogenised by grinding in liquid nitrogen. Fatty acid
169 methyl esters were separated on an HP-88 fused-silica capillary column (60 m X 0.25 mm i.d.,
170 0.2-µm film thickness, J & W 112-88A7, Agilent Technologies, USA) and quantified using a
171 fully automated 7890 Network GC System with a flame-ionization detector (Agilent). The
172 program setting details followed Jenkins' method [21]. C19:0 was used as the internal standard,
173 and the peaks were identified by comparison with FA standards (Sigma, 47885U and O5632).
174 The area percentage for all resolved peaks was analysed using GC ChemStation Software
175 (Agilent).

176 **2.11. Hepatic parameters measurements**

177 Hepatic tissues (0.1 g) were homogenised and resuspended in PBS solution. The
178 concentrations of total cholesterol (TC) and triglycerides (TGs) were respectively measured
179 using the corresponding detecting kits (Meimian Industrial Co. Ltd., China).

180 **2.12. Blood parameters measurements**

181 Unless otherwise stated, all blood samples were collected from the 11~15-week-old mice
182 fed ad libitum. Fresh blood from the tail veins was used to measure the circulating glucose
183 using a hand-held glucose monitor (Accu-Chek® Performa Blood Glucose Meter, Roche).
184 Heparin-treated blood from the tail vein was respectively used to measure the plasma TGs or
185 high-density lipoprotein (HDL) using a hand-held cholesterol monitor (On-Call® CCM-111
186 Blood Cholesterol System, Aikang Biotech Co. Ltd., China). Blood samples from the
187 submandibular vein of conscious mice were collected at the first 4~5 hrs of the light phase and
188 used to measure the serum corticosterone using the Cort ELISA kit (Ruixin Biotech Co. Ltd.,
189 China). Serums from the orbital sinus vein of anaesthetic mice were used to measure the
190 circulating TC, free fatty acids (FFA), prostaglandin E2 (PGE2) using the respective ELISA
191 kits (Meimian), as well as insulin, ghrelin, leptin, fibroblast growth factor 21 (FGF21),
192 interleukin-6 (IL-6), adrenaline glucagon tumour necrosis factor-alpha (TNFα), and C reactive
193 protein (CRP) using the respective ELISA kits (Ruixin).

194 **2.13. Intraperitoneally glucose tolerance test**

195 Mice fasted overnight were intraperitoneally injected with D-glucose (2 g/kg body
196 weight). Blood glucose was measured in a drop of blood collected from the tail vein before,
197 15, 30, 60, 90, and 120 min post glucose injection.

198 **2.14. Histological analysis**

199 Histological analysis was performed following the standard methods. Briefly, the tissues
200 were fixed by immersion in 4% formaldehyde in PBS and then dehydrated before embedding.
201 The 5-μm tissue sections (Leica CM1950) embedded with paraffin were dewaxed in xylene
202 and rehydration. Histological details were examined using hematoxylin-eosin staining kits

203 (Beijing Solarbio Science & Technology Co., Ltd., China). For red oil staining, 10-μm tissue
204 slices embedded by Tissue-Tek® O.C.T. Compound (Sakura, USA) were treated with a 60%
205 isopropyl alcohol solution twice, and histological details were examined after staining with oil
206 red O (Wuhan Servicebio Technology Co., Ltd., China). Stained slides were examined with an
207 Olympus microscope equipped with a digital camera.

208 Each cellular cross-sectional area was estimated following the method described by Chen
209 and Farese [22]. In detail, at least six slices from each mouse sample were randomly chosen
210 for image analysis. Firstly, three photos were randomly taken from non-overlapping
211 microscope fields of every slice under the 20 x objective. The cross-sectional area of each cell
212 on an image was calculated one by one using ImageJ software (Version 2.0.0), and the means
213 of the top 100 cell areas per picture represented the value of a microscope sampling field.
214 Finally, the means of at least 18 values per mouse sample (3 fields x 6 slices) were looked upon
215 as this sample's average cellular cross-sectional area for statistical analysis.

216 **2.15. Metabolic cage measurements**

217 Indirect calorimetry, heat production, and movement of 11-week-old mice were
218 measured using the Automated Home Cage Phenotyping TSE PhenoMaster V4.5.3 system
219 (TSE Systems Inc., Germany). The climate chamber was set to 22°C with a 12-h:12-h light-
220 dark cycle (lights on at 0700 h). Mice were individually housed in plexiglass cages and fed ad
221 libitum. VO_2, VCO_2, and food intake were measured every 39 min. After a 48 hrs acclimation
222 period, the data were collected for the following 72 hrs, and the calculated lean mass was
223 adjusted for all measurements.

224 **2.16. Statistical analysis**

225 All values are presented as mean ± SD. The statistical significance was assessed by
226 unpaired student's t-test or one-way ANOVA (Brown-Forsythe and Welch) among wt, pai/wt,
227 and pai/pai mice. A value of $p < 0.05$ was considered statistically significant.

228

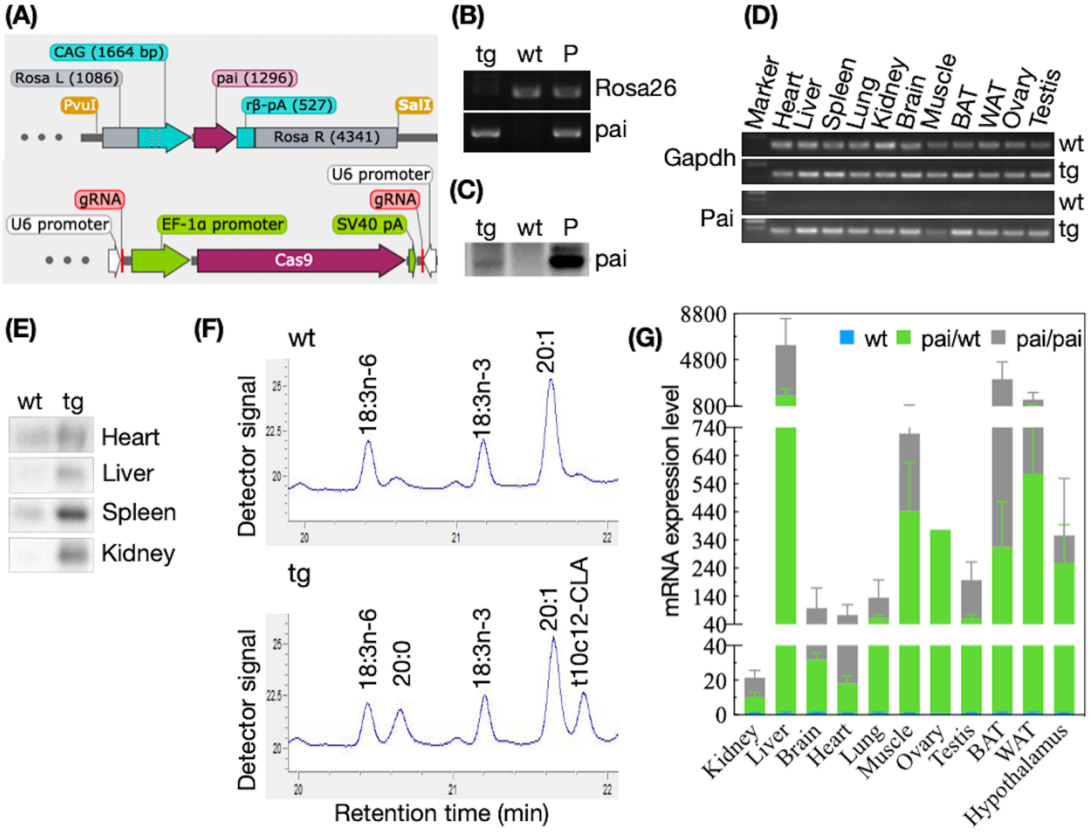

Figure 1. Transgene analysis. (A) Strategy for inserting the pai-expressing cassette into the Rosa26 locus by the CRISPR/Cas9 technique. The upper panel illustrates the recombined homological vector in which the codon-optimised Pai gene is driven by a CAG promoter and ended by a rabbit beta-globin polyA signal (rβ-pA). Rosa L and Rosa R represent the left and right sequences of the insertional site within the first intron of Rosa26, respectively. Linear DNA fragments digested with Pvu I and Sal I enzymes are used for co-microinjection. The down panel shows the CRISPR/Cas9 plasmid containing EF-1α-driven Cas9 and dual gRNA target sequences for co-microinjection. The numbers in brackets indicate the sequence length. (B) PCR and (C) Southern blot analysis of the genomic DNA samples from transgenic (tg), wild-type (wt) mice, and wt DNA mixed with a pRosa-Pai plasmid (P) shows that the Pai gene is inserted into

the Rosa26 locus in the tg sample. PCR products are 514-bp fragments spanning the Pai gene and 605-bp fragments spanning the insertional site of the Rosa26 sequence. (D) RT-PCR analysis of RNAs shows that the Pai gene is expressed in all tg tissues, including brown (BAT) and white (WAT) adipose tissues, not in all wt samples. The amplified product of Pai is 164-bp fragments, and the Gapdh is 78-bp fragments as an internal control. (E) Western blot analysis reveals that PAI antigen existed in the tg heart, liver, spleen, and kidney, not in wt samples. (F) The lipid profiles of partial gas chromatography traces show that the t10c12-CLA is produced in the kidney of the tg mouse compared to its wt littermate. (G) Real-time PCR analysis showed that the relative mRNA expression level of the Pai gene is quite different in each sample from biallelic pai/pai or monoallelic pai/wt mice (n=3), and no Pai mRNA is detected in samples of their wt littermates. Each value represents the mean ± SD after normalisation to the mRNA levels of Gapdh.

229 # 3. Results

230 ## 3.1. Transgene analysis

231 The strategy to insert the pai-expressing cassette into the Rosa26 locus is shown in Figure
232 1A. PCR and Southern blot (Fig. 1 B-C) and DNA sequencing analysis demonstrated that the
233 correct transgene was inserted into the Rosa26 locus in a founder mouse among 96 mice
234 derived from injected embryos. RT-PCR and western blot analyses (Fig. 1 D-E) indicated that
235 the pai gene was expressed in all tested tissues. Gas chromatography verified that the functional
236 PAI enzyme produced the t10c12-CLA successfully (Fig. 1 F). Real-time PCR analysis (Fig.
237 1 G) revealed that the mRNA levels of Pai were quite different between biallelic pai/pai and
238 monoallelic pai/wt mice; thus, two pai genotypes were analysed separately in the following
239 tests.

240 ## 3.2. Fatty acids analysis

241 T10c12-CLA and FAs compositions in the hearts, livers, kidneys, tibialis anterior
242 muscle, BAT, or WAT were analysed by gas chromatography. Compared to wt littermates, the
243 contents (μg/g of tissue weight) of t10c12-CLA had increased in the kidneys ($p = 0.004$) and
244 heart ($p = 0.055$) from pai/wt mice and WAT from pai/wt or pai/pai mice ($p < 0.05$; Table 1),
245 not in the other examined tissues, suggesting that the t10c12-CLA is produced in trace amounts
246 or degraded quickly. Simultaneously, the quantities of LA substrates had decreased in the livers
247 from both pai genotypes and increased in the pai/wt kidneys ($p < 0.05$; Table 1).

248 The contents of other FAs, such as myristic (14:0), palmitic (16:0), palmitoleic (16:1n-
249 7), stearic (18:0), oleic (18:1n-9), cis-vaccenic (18:1n-7), or arachidonic (20:4n-6) acids, were
250 changed by varying degrees in pai heart, kidney, liver or WAT tissues (Supplementary Table

Table 1. Contents of t10c12-CLA and linoleic acid in wt and pai mice

	T10c12-CLA (μg/g)			Linoleic acid (mg/g)		
	wt (n)	pai/wt (n)	pai/pai (n)	wt (n)	pai/wt (n)	pai/pai (n)
Heart	7.12 ± 0.95 (11)	8.85 ± 1.20 (8)	8.47 ± 2.35 (8)	2.06 ± 0.31 (11)	2.03 ± 0.31 (8)	2.11 ± 0.19 (8)
Liver	11.93 ± 8.27 (12)	16.65 ± 12.53 (11)	9.93 ± 1.31 (10)	1.29 ± 0.20[a] (12)	1.09 ± 0.25[b] (11)	1.07 ± 0.23[b] (10)
Kidney	6.77 ± 1.16[a] (12)	11.33 ± 4.18[b] (13)	6.87 ± 1.17[a] (8)	1.13 ± 0.16[a] (10)	1.38 ± 0.26[b] (13)	1.20 ± 0.19[a] (8)
Muscle	ND (9)	ND (8)	ND (8)	0.87 ± 0.41 (9)	0.84 ± 0.31 (8)	0.61 ± 0.17 (8)
BAT	25.87 ± 16.37 (8)	25.63 ± 10.00 (8)	28.80 ± 7.52 (7)	1.88 ± 0.31 (8)	1.70 ± 0.42 (8)	1.69 ± 0.31 (7)
WAT	ND (5)	4.10 ± 1.05 (3)	4.89 ± 0.83 (3)	0.50 ± 0.34[ab] (5)	0.33 ± 0.01[a] (3)	0.44 ± 0.01[b] (3)

Note: Tissues of mice at the age of 11 weeks are used for gas chromatography, and 19:0 is an internal standard. ND, Not detected. Each value represents the mean ± SD, and the numbers in brackets indicate the size of the tested samples. For all fatty acid contents, see Supplementary Table 4. Different letters in superscript indicate a level of statistical significance of $p < 0.05$.

251 4). In contrast, no evident changes in FA compositions were observed in pai muscle and BAT
252 tissue, suggesting the content changes of some FAs are genotype- or tissue-specific.
253 Simultaneously, the amounts of total FAs were decreased in the pai/pai livers (9.19 ± 1.55 in
254 wt versus 8.19 ± 1.78 mg/g in pai/pai; $p < 0.05$) and contrarily increased in both pai kidneys
255 (9.59 ± 0.99 in wt versus 12.97 ± 2.21 in pai/wt versus 10.66 ± 1.06 in pai/pai; $p < 0.05$;
256 Supplementary Table 4), suggesting fat loss in livers but fat accumulation in kidneys.

257 **3.3. Weaning and growth analysis**

258 Considering the potential impact of maternal t10c12-CLA from the placenta and/or milk,
259 pups delivered by wt or pai/wt mothers were measured separately. In the group of wt mothers
260 (Fig. 2A), the pai/wt pups showed no bodyweight difference from the wt littermates during the
261 post-weaning development. In the group of pai/wt mothers (Fig. 2B), the pai/wt or pai/pai pups
262 also showed no bodyweight difference from the wt littermates during the post-weaning
263 development. However, the pai/wt genotypes were overweight ($p < 0.05$) than pai/pai mice
264 from 10 weeks onwards.

265 Interestingly, within the group of pai/wt mothers, the weaning weights of three genotypes
266 were significantly different (pai/pai < pai/wt < wt, respectively; $p < 0.05$. Fig. 2 B-C),
267 suggesting the endogenous t10c12-CLA produced by foetus/pups themselves would result in
268 the reduced bodyweight during embryonic/weaning development. On the other hand, the
269 weaning weights of wt or pai/wt pups from pai/wt mothers were respectively overweight than
270 that from wt mother ($p < 0.05$; Fig. 2C), suggesting that the maternal t10c12-CLA might result
271 in the increased bodyweight of the embryos/pups.

272 **3.4. Energy metabolism and activity studies**

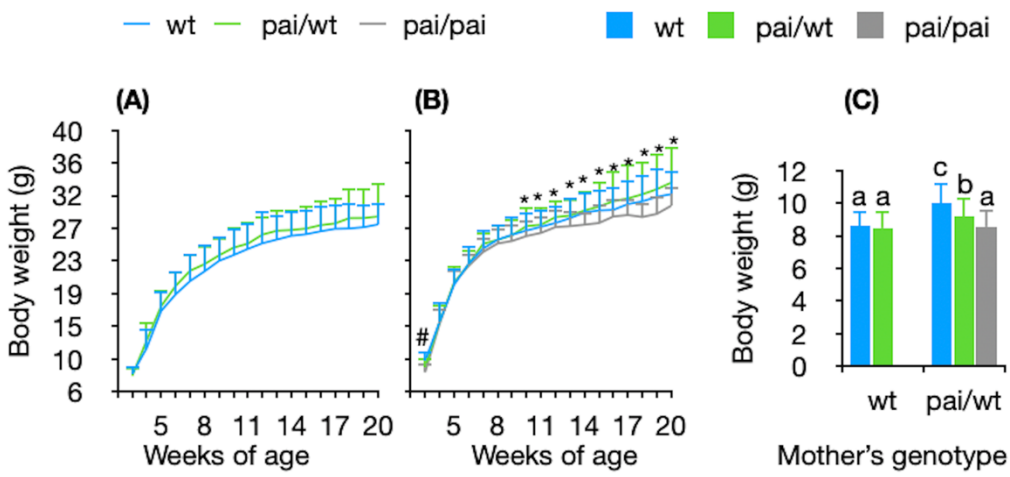

Figure 2. Growth curves of different genotype pups from wt (A) or pai/wt (B) mother and comparison of the body weight (C) of pups at the age of 3 weeks. Each group contained 15-20 (A, B) or 30-85 (C) pups. Bars represent the mean ± SD. # and different letters indicate $p < 0.05$ among three genotypes; * indicates $p < 0.05$ between pai/pai and pai/wt genotypes.

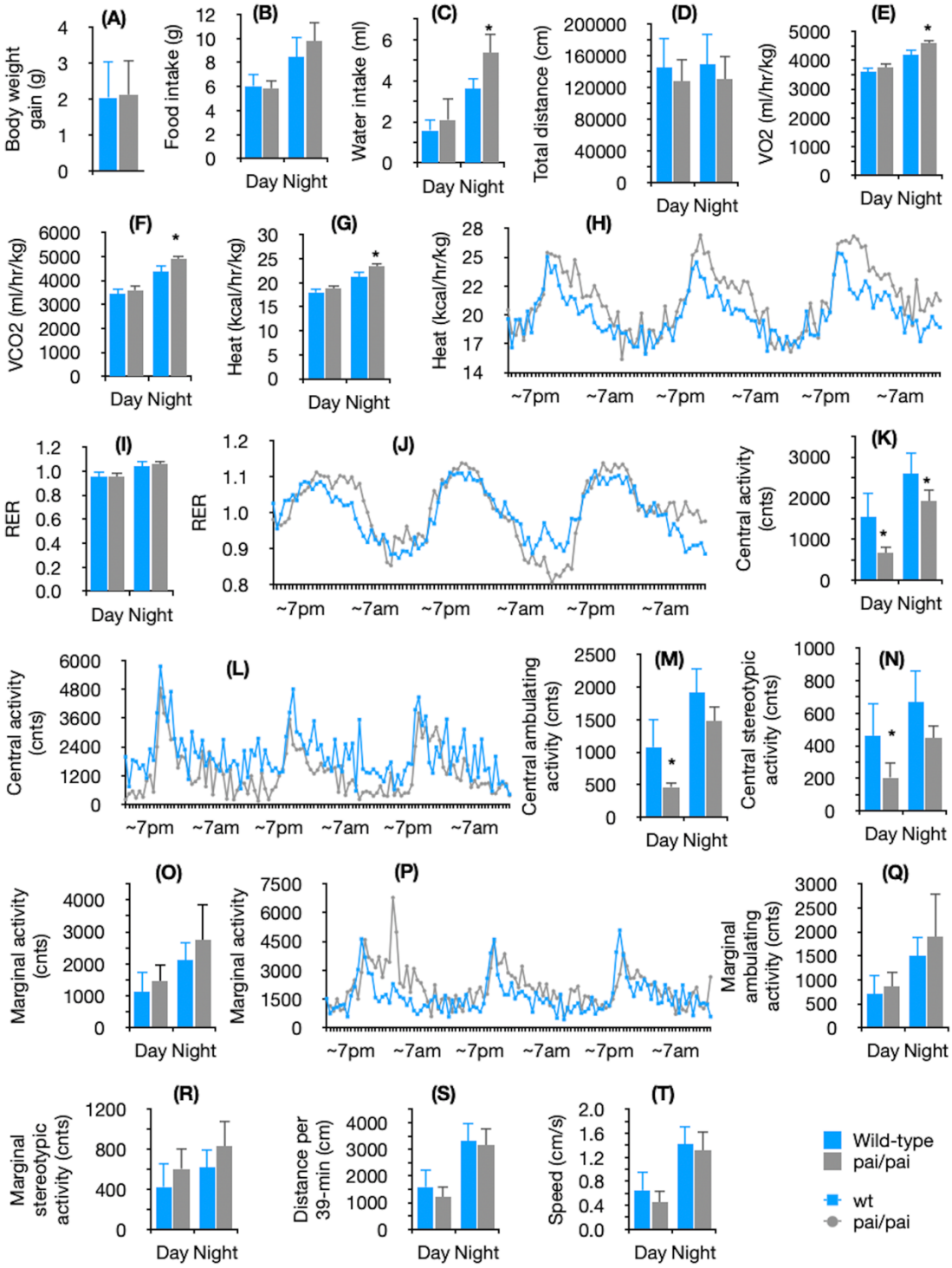

Figure 3. Pai mice have abnormal energy metabolism and activities. Comparison of body weight gain during 72 h period (A), food intake (B), water intake (C), total distance travelled during 72 h period (D), O_2 consumption (E), CO_2

production (F), heat release and its time course (G-H), respiratory exchange ratio (REF) and RER time course (I-J), locomotor activities in the centre of the cage and its time course (K-L), central ambulating and stereotypic activities (M-N), locomotor activities in the margin or corners of the cage and its time course (O-P), marginal ambulating and stereotypic activities (Q-R), distance travelled during a 39-min sampling duration (S), and speed (T) among wt (n=5) and pai/pai (n=5) mice at the age of 11 weeks. Lights turn on and off at 7:00 am and 7:00 pm, respectively. The data are normalised to lean body weight. Bars represent the mean ± SD. * indicate $p < 0.05$ within the same phase.

273 Energy metabolism and activity parameters were determined under the consideration of
274 body weight in the 11-week-old pai/pai mice and wt littermates over 72 hrs in metabolic cages
275 (Fig. 3). Compared to the wt littermates, pai/pai mice showed no different ($p > 0.05$) changes
276 in food intake, respiratory exchange ratio, marginal activities, and speed in both light and dark
277 phases; as well as body weight gain and total distance travelled during the 72 hrs period.

278 However, pai/pai mice had fewer central activities significantly ($p < 0.05$) in both light
279 (56%) and dark (26%) phases, but they consumed 32% and 48% more water, 4.1% and 9.9%
280 more O_2, and produced 4.3% and 12% more CO_2, and 4.2% and 10.4% more heat during the
281 light ($p > 0.05$) and dark ($p < 0.05$) periods, respectively (Fig. 3). That was, pai/pai mice
282 reduced their activities, but consumed more oxygen (energy) to release more heat for
283 maintenance.

284 **3.5. Metabolic complications**

285 To match energy demand and expenditure, the circulating hormonal signals were
286 examined under the non-fasted state. The concentrations of serum insulin, leptin, ghrelin, and
287 circulating glucose (Table 2), as well as the length of the small intestine (Supplementary Table
288 5), showed no differences ($p > 0.05$) among the three genotypes. It suggests that the t10c12-
289 CLA does not play a role in the energy intake, consistent with the observation in the metabolic
290 cage.

291 Glucose tolerance tests showed no difference in the circulating glucose concentrations or
292 the area under the curve among the three genotypes (Fig. 4 A). However, the blood glucose
293 levels before glucose injection were remarkably ($p < 0.05$; Fig. 4 A) increased in pai/wt mice
294 and maintained typically when fasted 24-h duration (Fig. 4 B). It suggests that the t10c12-CLA
295 might ameliorate the glucose sensitivity in pai/wt mice at the beginning of starvation, which

Table 2. Hormones/factors in blood in wt and pai mice

	wt (n)	pai/wt (n)	pai/pai (n)
Serum total cholesterol (μM)	304 ± 32 (12)	303 ± 44 (9)	301 ± 50 (8)
Plasma triglycerides (mg/dL)	126 ± 27[a] (33)	107 ± 30[b] (30)	110 ± 28[b] (30)
Plasma high-density lipoprotein (mg/dL)	68.5 ± 17.0 (36)	71.3 ± 19.1 (30)	66.7 ± 17.9 (31)
Serum free fatty acids (μM)	407 ± 125 (14)	394 ± 90 (19)	465 ± 110 (10)
Blood glucose (mM)	7.98 ± 1.44 (28)	8.45 ± 0.92 (22)	7.95 ± 1.32 (26)
Serum insulin (μg/L)	0.41 ± 0.06 (12)	0.41 ± 0.08 (8)	0.44 ± 0.12 (9)
Serum leptin (μg/L)	1.05 ± 0.48 (12)	1.15 ± 0.47 (13)	1.21 ± 0.55 (11)
Serum ghrelin (ng/L)	184 ± 27 (7)	216 ± 56 (8)	194 ± 19 (9)
Serum fibroblast growth factor 21 (ng/L)	441 ± 38[a] (15)	480 ± 43[b] (12)	423 ± 27[a] (15)
Serum prostaglandin E2 (ng/L)	342 ± 42 (15)	327 ± 31 (9)	337 ± 42 (14)
Serum glucagon (mU/L)	75.1 ± 53.5 (14)	78.8 ± 51.4 (14)	103 ± 62 (13)
Serum cortosterone (μg/L)	9.03 ± 2.56 (16)	9.44 ± 2.44 (8)	9.44 ± 2.49 (16)
Serum adrenaline (μg/L)	4.56 ± 4.34 (11)	3.51 ± 3.06 (18)	6.30 ± 5.53 (5)
Serum interleukin-6 (ng/L)	17.3 ± 16.1 (8)	22.3 ± 23.5 (15)	23.7 ± 12.2 (9)
Serum tumour necrosis factor α (ng/L)	157 ± 139 (20)	249 ± 168 (12)	184 ± 181 (11)
Serum C reactive protein (μg/L)	20.1 ± 14.1 (9)	17.9 ± 15.8 (7)	34.0 ± 41.4 (11)

Note: Blood samples were collected from non-fasted mice at the ages of 11~15 weeks. Each value represents the mean ± SD, and the numbers in brackets indicate the size of the tested samples. Different letters in superscript indicate a level of statistical significance of $p < 0.05$.

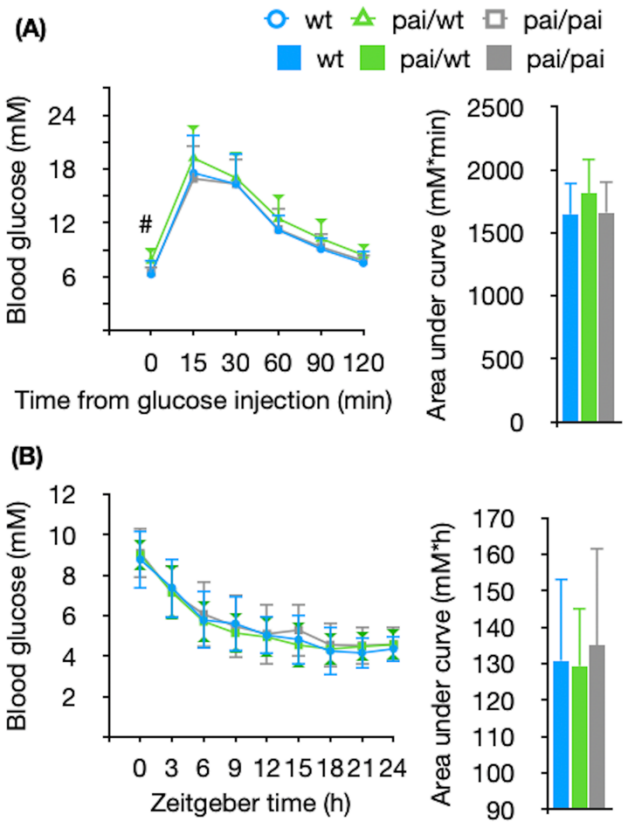

Figure 4. Blood glucose tolerance test and dynamic glucose levels in wt and pai mice. (A) Comparison of glucose tolerance and the area under curve among wt and pai mice. (C) Dynamic blood glucose changes in fasting mice starved from Zeitgeber time 0 to 24. Zeitgeber times 0 and 12 are defined as lights-on and -off times, respectively. Bars represent the mean ± SD. # indicates $p < 0.05$ between pai/wt with wt or pai/pai mice.

296 may be associated with the elevated FGF21 in pai/wt mice ($p < 0.05$; Table 2) for FGF21 plays
297 an active role in insulin-sensitising and energy expenditure [23].

298 In addition, there were no differences in the circulating TC, FFAs, and HDL among the
299 three genotypes, but the serum levels of TGs were reversely decreased in pai/wt ($p = 0.011$) or
300 pai/pai mice ($p = 0.021$; Table 2) compared to wt mice.

301 Furthermore, the serum PGE2, glucagon, corticosterone, adrenaline, TNFα, IL-6, and
302 CRP in pai/wt or pai/pai mice were respectively kept at normal levels compared with wt mice
303 ($p > 0.05$; Table 2), suggesting no pathological symptoms such as cellular toxicity of expressing
304 the bacterial protein, response to illness-related stimuli, and inflammation in pai mice. It also
305 indicates that the phenotype profiling of pai mice is just a result of the t10c12-CLAs' impact.

306 **3.6. WAT reduction**

307 Mice at 11 weeks were used to determine the WAT features by dissection, magnetic
308 resonance (MR) imaging, histological, and RNA analyses. The results exhibited genotype-
309 specific and described as follows. Compared to wt mice, in pai/wt mice, no evident changes in
310 organs/tissues, adipocyte volume or cross-sectional areas per adipocyte (Fig. 5 B-D) were
311 observed. On the contrary, in pai/pai mice, organs such as livers, spleens, and kidneys were
312 significantly enlarged ($p < 0.05$; Supplementary Table 5). Simultaneously, the white fat was
313 lost (Fig. 5 A-B), consistent with the reduced adipocyte volume or cross-sectional areas per
314 adipocyte (Fig. 5 C-D), as well as the lowered RNA levels of leptin, Cebpβ (Full name seen in
315 Table 3) that plays a role in the early stages of adipogenesis, macrophage markers F4/80, CD68,
316 and CD11c in WAT (Table 3). The results suggest that the t10c12-CLA can result in fat loss
317 in pai/pai mice.

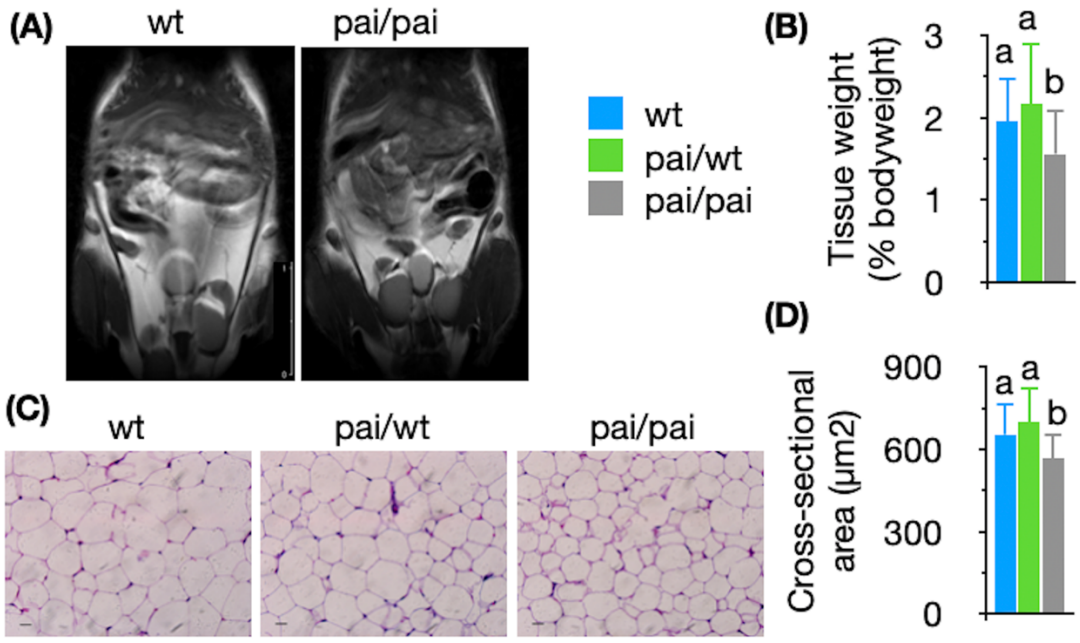

Figure 5. Magnetic resonance imaging and histological analysis of white adipose tissues. (A) Coronal sections were obtained on the whole-body midsection for five wt or pai/pai mice at 11 weeks in each group during magnetic resonance imaging (bar = 1 cm). The wt mice show adipose tissue in the subcutaneous and intra-abdominal regions as areas of increased signal intensity on images. The pai/pai mice show less fat. (B) The WAT weight and (C) Imaging by hematoxylin-eosin staining (bar = 10 μm), as well as (D) analysis of cross-sectional area per adipocyte, show that the volumes of white adipocytes are reduced in pai/pai mice. Bars represent the mean ± SD. Different letters indicate $p < 0.05$.

Table 3. Relative expression of mRNAs in the white (WAT) and brown (BAT) adipose tissues

	WAT		BAT	
Genes	wt (n)	pai/pai (n)	wt (n)	pai/pai (n)
Fatty acid synthase (*Fasn*)	1.01 ± 0.32 (22)	4.70 ± 2.25*** (28)	0.99 ± 0.30 (15)	1.61 ± 0.58** (16)
Peroxisome proliferator-activated receptor-γ (*Ppar-γ*)	1.04 ± 0.28 (17)	1.01 ± 0.46 (12)	1.01 ± 0.18 (13)	1.41 ± 0.26*** (15)
Adipose triglyceride lipase (*Atgl*)	1.08 ± 0.45 (7)	0.69 ± 0.07 (5)	1.07 ± 0.45 (7)	0.76 ± 0.44 (8)
Hormone-sensitive lipase (H*sl*)	1.04 ± 0.30 (7)	0.82 ± 0.06 (5)	1.05 ± 0.35 (8)	0.58 ± 0.23** (8)
Monoacylglycerol lipase (*Mgl*)	1.06 ± 0.41 (8)	1.05 ± 0.19 (6)	1.04 ± 0.30 (8)	0.54 ± 0.24** (8)
Perilipin 1a	1.03 ± 0.28 (7)	0.95 ± 0.16 (6)	1.15 ± 0.62 (8)	0.61 ± 0.15* (7)
Comparative gene identification 58 (*Cgi58*)	1.03 ± 0.26 (8)	1.16 ± 0.49 (7)		
Lipoprotein lipase (*Lpl*)	1.01 ± 0.12 (12)	0.59 ± 0.24*** (12)	1.00 ± 0.26 (15)	0.69 ± 0.27** (14)
Carnitine palmitoyltransferase 1a (*Cpt1a*)	1.08 ± 0.45 (7)	1.60 ± 1.13 (8)	1.03 ± 0.26 (8)	0.68 ± 0.28* (7)
Carnitine palmitoyltransferase 1b (*Cpt1b*)			1.04 ± 0.33 (7)	0.42 ± 0.21** (8)
Long-chain 3-hydroxyacyl-CoA dehydrogenase (*Lchad*)	1.05 ± 0.34 (8)	1.16 ± 0.47 (7)		
Acetyl-CoA acyltransferase 2 (*Acaa2*)	1.03 ± 0.28 (8)	1.66 ± 0.59* (7)		
Long-chain acyl-CoA dehydrogenase (*Lcad*)	1.04 ± 0.32 (17)	1.69 ± 0.65** (16)	1.01 ± 0.13 (13)	0.99 ± 0.48 (14)
Medium-chain acyl-CoA dehydrogenase (*Mcad*)	1.05 ± 0.38 (8)	1.18 ± 0.39 (8)	1.01 ± 0.20 (6)	1.04 ± 0.37 (7)
Uncoupling protein 1 (*Ucp1*)	0.97 ± 0.34 (8)	0.59 ± 0.36* (10)	1.04 ± 0.29 (18)	0.65 ± 0.29*** (22)
Uncoupling protein 2 (*Ucp2*)	1.04 ± 0.38 (12)	0.31 ± 0.22*** (13)	1.01 ± 0.14 (9)	0.64 ± 0.15*** (8)
Ppar-gamma coactivator 1 alpha (*Pgc1*α)	1.04 ± 0.31 (8)	1.94 ± 0.42** (5)	1.04 ± 0.31 (6)	1.63 ± 0.53* (7)
PR domain containing 16 (*Prdm16*)	1.02 ± 0.24 (6)	0.65 ± 0.21* (7)	1.04 ± 0.28 (7)	1.20 ± 0.55 (8)
Sterol regulatory element binding protein-1a (*Srebp1a*)	1.05 ± 0.33 (13)	0.98 ± 0.48 (8)	1.03 ± 0.25 (5)	0.61 ± 0.15* (5)
Sterol regulatory element binding protein (*Srebp2*)	1.03 ± 0.42 (12)	0.99 ± 0.40 (13)	1.01 ± 0.19 (5)	1.46 ± 0.81 (4)

Table 3. Relative expression of mRNAs in the white (WAT) and brown (BAT) adipose tissues

	WAT		BAT	
Genes	wt (n)	pai/pai (n)	wt (n)	pai/pai (n)
Insulin receptor	1.03 ± 0.25 (7)	1.15 ± 0.38 (8)		
Insulin receptor substrate-1 (*Irs1*)	1.00 ± 0.31 (23)	0.50 ± 0.21*** (17)		
Insulin receptor substrate-2 (*Irs2*)	1.12 ± 0.54 (8)	1.09 ± 0.50 (8)		
Phosphoinositide 3-kinase (*Pi3k*)	1.06 ± 0.36 (6)	5.11 ± 3.08* (6)		
Insulin-like growth factor-1 (*Igf1*)	1.05 ± 0.34 (8)	0.85 ± 0.32 (7)		
IGF binding protein 1 (*Igfbp1*)	1.19 ± 0.66 (6)	1.08 ± 0.42 (6)		
Glucose-6-phosphate dehydrogenase (*G6pd*)	0.97 ± 0.23 (13)	0.99 ± 0.68 (10)	1.01 ± 0.13 (5)	1.48 ± 1.02 (5)
Glucose transporter type 4 (*Glut4*)	1.01 ± 0.15 (18)	0.45 ± 0.26*** (18)	1.01 ± 0.18 (4)	3.15 ± 0.76** (4)
Carbohydrate response element binding protein (*Chrebp*)	0.98 ± 0.25 (12)	1.84 ± 0.78** (11)	1.02 ± 0.20 (5)	0.88 ± 0.33 (5)
Fibroblast growth factor 21 (*Fgf21*)	1.04 ± 0.32 (7)	1.10 ± 0.33 (7)		
Glucose-6-phosphatase (*G6p*)	0.96 ± 0.38 (16)	0.39 ± 0.17*** (24)		
Phosphoenolpyruvate carboxykinase (*Pepck*)	1.08 ± 0.39 (8)	1.04 ± 0.67 (7)		
AMP-activated protein kinase (*Ampk)*	1.02 ± 0.35[a] (15)	1.41 ± 0.57* (15)	1.01 ± 0.17 (8)	2.24 ± 1.46* (8)
Leptin	1.01 ± 0.16 (6)	0.34 ± 0.12*** (7)		
Adiponecin	1.03 ± 0.28 (8)	0.87 ± 0.28 (11)		
Nuclear receptor subfamily 3 group C member 1 (*Nr3c1*)	1.02 ± 0.23 (8)	0.94 ± 0.39 (8)		
F4/80	1.04 ± 0.30 (28)	0.50 ± 0.27*** (30)		
CD68	1.00 ± 0.34 (31)	0.48 ± 0.31*** (36)		
CD11c	1.04 ± 0.32 (17)	0.34 ± 0.27*** (20)		
Acyl-CoA-binding protein (A*cbp*)	1.02 ± 0.20 (9)	0.67 ± 0.20** (8)	1.00 ± 0.08 (5)	1.02 ± 0.39 (5)

Table 3. Relative expression of mRNAs in the white (WAT) and brown (BAT) adipose tissues

	WAT		BAT	
Genes	wt (n)	pai/pai (n)	wt (n)	pai/pai (n)
CCAAT/enhancer-binding-protein beta (*Cebpβ*)	1.05 ± 0.37 (6)	0.58 ± 0.34* (8)		
Pai	0.99 ± 0.50 (14)	1320 ± 622*** (19)	1.08 ± 0.45 (8)	3108 ± 1504*** (9)

Numbers in brackets of the parameters indicate the size of tested samples. Each value represents the mean ± SD. * indicates $p < 0.05$; ** indicates $p < 0.01$; *** indicates $p < 0.001$ within the same tissue, respectively.

318 In pai/pai white adipocytes, significant ($p < 0.05$) changes in RNA levels appeared in
319 50% (20/40) tested genes, including seven up-regulated and 13 down-regulated (Table 3). The
320 energy regulator Ampk was up-regulated, suggesting the inhibition of lipid synthesis, which is
321 consistent with the down-regulated lipoprotein lipase that supports the uptake of FAs from very
322 low-density lipoproteins in the bloodstream, regular expression of Srebp1a and Srebp2
323 involved in the sterol pathway and transcriptional factor Ppar-γ, while the fatty acid synthase
324 over-expressed. Genes involved in lipolyses, such as Atgl, hormone-sensitive lipase, Mgl,
325 Perilipin 1a, and Ggi58 kept normal RNA levels. Normal RNA levels of genes involved in
326 beta-oxidation, including Cpt1a, Lchad, and Mcad and the reduced RNA levels of the acyl-
327 CoA-binding protein that act as an intracellular carrier of acyl-CoA esters were detected in
328 pai/pai WAT, suggesting the weakening, not enhancing the process of beta-oxidation in
329 mitochondria. On the contrary, the RNA levels of Acaa2 and Lcad were increased, suggesting
330 the up-regulation of beta-oxidation of very long-chain FAs in peroxisomes.

331 In pai/pai adipocytes, although Pgc1α, which activates mitochondrial biogenesis genes
332 through interaction with Ppar-γ during energy stress, were up-regulated. Simultaneously,
333 Prdm16, Ucp1, and Ucp2 were down-regulated, suggesting the declined WAT browning.

334 Consistent with the normal levels of the circulating insulin or glucocorticoids, their
335 receptor genes Insr and Nr3c1, also expressed commonly on the pai/pai adipocyte surface;
336 interestingly, the Irs1 was down-regulated while its downstream Pi3K gene was up-regulated.
337 The RNA levels of other genes involved in insulin/IGF-1 signalling, such as Irs2, Igf1, and
338 Igfbp1 had no changes compared to the wt samples. Meanwhile, reduced expression of Chrebp
339 and glucose transporter Glut4, as well as up-regulated glucose-6-phosphatase involved in
340 gluconeogenesis, suggesting the energy mobilisation for glucose homeostasis. These results

341 indicate that the t10c12-CLA has induced the broadly positive or negative feedback regulation
342 of lipid and glucose metabolism in WAT.

343 **3.7. BAT thermoregulation**

344 Parameters of BAT were measured to investigate the molecular mechanism of more heat
345 production in pai mice. MR imaging and dissection analysis revealed that the weight (%
346 bodyweight) of interscapular BAT was increased from 0.39 ± 0.07 in wt to 0.50 ± 0.18 in pai/wt
347 ($p = 0.059$) and 0.54 ± 0.18 in pai/pai mice ($p < 0.05$; Fig. 6 A-C). HE staining showed that
348 there were more small-sized and irregular lipid drops within the pai/wt or pai/pai adipocytes,
349 quite different from the wt adipocytes containing relatively uniform and medium-sized lipid
350 drops (Fig. 6 D); simultaneously, the size of cross-sectional area per brown adipocyte was
351 enlarged in both pai genotypes ($p < 0.05$; Fig. 6 E). It suggests that t10c12-CLA-induced BAT
352 mass increased in pai mice.

353 RNA sequencing was performed to provide a snapshot of the transcriptional dynamics
354 between the wt and pai/pai BAT. The heatmap (Fig. 6 F) and a volcano plot (Fig. 6 G) revealed
355 that the global transcriptional profile of pai/pai BAT differed from that of wt BAT. KEGG
356 pathway enrichment analysis showed that the up-regulated pathways in pai/pai BAT included
357 fatty acid biosynthesis, pyruvate metabolism, carbohydrate digestion and absorption, Insulin
358 signalling pathway, steroid biosynthesis, biosynthesis of amino acids, citrate cycle, and
359 propanoate metabolism (Fig. 6 H). In contrast, the down-regulated pathway included NK cell-
360 mediated cytotoxicity, C-type lectin receptor signalling pathway, cell adhesion molecules,
361 phagosome, tuberculosis, Fc epsilon RI signalling pathway, adherens junction, antigen
362 processing and presentation, and Fc gamma R-mediated phagocytosis signalling pathways
363 (Fig. 6 I).

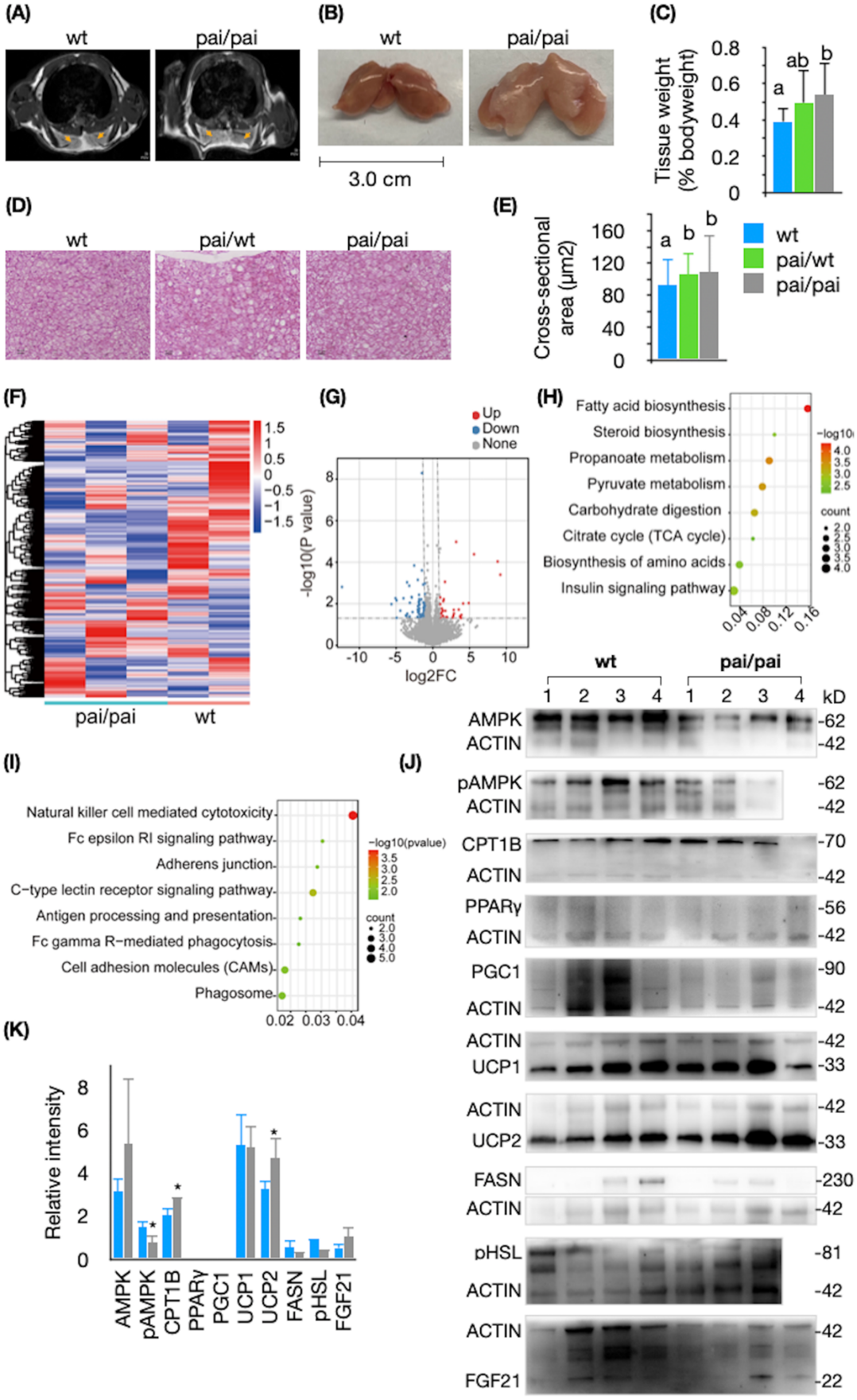
(A)
wt
pai/pai
(B)
wt
pai/pai
3.0 cm
(C)
Tissue weight (% bodyweight)
0.8
0.6
0.4
0.2
0
a
ab
b
(D)
wt
pai/wt
pai/pai
(E)
Cross-sectional area (μm2)
160
120
80
40
0
a
b
b
wt
pai/wt
pai/pai
(F)
1.5
1
0.5
0
−0.5
−1
−1.5
pai/pai
wt
(G)
Up
Down
None
-log10(P value)
log2FC
(H)
Fatty acid biosynthesis
Steroid biosynthesis
Propanoate metabolism
Pyruvate metabolism
Carbohydrate digestion
Citrate cycle (TCA cycle)
Biosynthesis of amino acids
Insulin signaling pathway
−log10
count
(I)
Natural killer cell mediated cytotoxicity
Fc epsilon RI signaling pathway
Adherens junction
C−type lectin receptor signaling pathway
Antigen processing and presentation
Fc gamma R−mediated phagocytosis
Cell adhesion molecules (CAMs)
Phagosome
−log10(pvalue)
count
(J)
wt
pai/pai
1 2 3 4 1 2 3 4
kD
AMPK
ACTIN
-62
-42
pAMPK
ACTIN
-62
-42
CPT1B
ACTIN
-70
-42
PPARγ
ACTIN
-56
-42
PGC1
ACTIN
-90
-42
ACTIN
UCP1
-42
-33
ACTIN
UCP2
-42
-33
FASN
ACTIN
-230
-42
pHSL
ACTIN
-81
-42
ACTIN
FGF21
-42
-22
(K)
Relative intensity
AMPK
pAMPK
CPT1B
PPARγ
PGC1
UCP1
UCP2
FASN
pHSL
FGF21

Figure 6. Aspects of brown adipose tissues. Axial sections of the interscapular BAT show more prominent areas of grey signal intensity on magnetic resonance images (Brown arrows) in five pai/pai mice than that in five wt mice at the age of 11 weeks (A). The BAT mass increases in pai/pai mice (B, C). Imaging by hematoxylin-eosin staining show more small-sized and irregular lipid drops in the pai/wt or pai/pai adipocytes and relatively uniform and medium-sized lipid drops in the wt adipocytes (D, bar = 10 μm) and analysis of cross-sectional area per cell show that the volumes of brown adipocytes are increased in pai mice (E). RNA-Seq analysis shows transcriptional changes of differentially expressed genes in BAT from two wt and three pai/pai mice using heatmap (F) and the up- or down-regulated genes in pai/pai BAT using volcano plots (G). Maps of KEGG enrichment analysis show the up- (H) and down-regulated (I) metabolic pathways in pai/pai BAT. Western blot images (J) and relative intensities (K) analyses of some critical proteins in the BAT from wt and pai/pai mice. ACTIN, beta-actin; (p)AMPK, (phosphorylated) AMP-activated protein kinase; CPT1B, carnitine palmitoyltransferase 1b; FASN, fatty acid synthase; FGF21, fibroblast growth factor 21; PGC1α, pparγ coactivator 1α; pHSL, phosphorylated hormone-sensitive lipase; PPARγ, peroxisome proliferator-activated receptor-γ; UCP, uncoupling protein. Bars represent the mean ± SD. Different letters in superscript or * indicate $p < 0.05$.

364 Based on the prediction of transcriptome analysis and the conventional physiological
365 factors that can impact BAT's activity, 24 genes were chosen for real-time PCR analysis and
366 fourteen (56%) of them altered their transcriptional patterns in pai/pai brown adipocytes.
367 Among them, five up-regulated genes were Ampk, Fasn, Glut4, Ppar-r, and Pgc1α and nine
368 down-regulated genes were Srebp1a, Lpl, Hsl, Mgl, Perilipin1a, Cpt1a, Cpt1b, Ucp1, and Ucp2
369 (Table 3). In addition, western blot analysis revealed that the protein level of AMPK was not
370 altered. In contrast, the pAMPK level was increased significantly in pai/pai BAT compared
371 with the wt samples (Fig. 6 J-K), suggesting the AMPK activation to rewire metabolism to
372 decrease anabolic processes and increase catabolism. Coordinately, the elevation of CPT1B
373 and UCP2 proteins suggests the increased lipid beta-oxidation and BAT thermogenesis in
374 pai/pai mice. However, no difference in protein levels of UCP1, PGC1, FASN, PPAR-γ, pHSL,
375 and FGF21 in the samples of BAT from the pai/pai and wt mice (Fig. 6 J-K). The inconsistency
376 between some RNA and protein levels suggests the possibility of feedback regulation in pai
377 mice.

378 **3.8. Hepatic features**

379 Compared to wt mice, the hepatic analysis also showed varying degree differences
380 between pai/wt and pai/pai livers. Besides liver hypertrophy ($p < 0.05$; Fig. 7 A) and the amount
381 decrease of total FAs ($p < 0.05$; Supplementary Table 4) in pai/pai livers, the hepatic TC or
382 TGs levels had not changed ($p > 0.05$; Fig. 7 B-C), and no steatosis was observed by
383 histological staining of liver slices from pai/wt and pai/pai mice, while the estimation of cross-
384 sectional area per cell showed hepatocytes were swollen (Fig. 7 D-G), consistent with liver
385 hypertrophy in both pai genotypes. In addition, the mRNA levels of 58% (28/48) critical genes
386 were significantly changed in pai/pai livers, including 11 down-regulated and 17 up-regulated

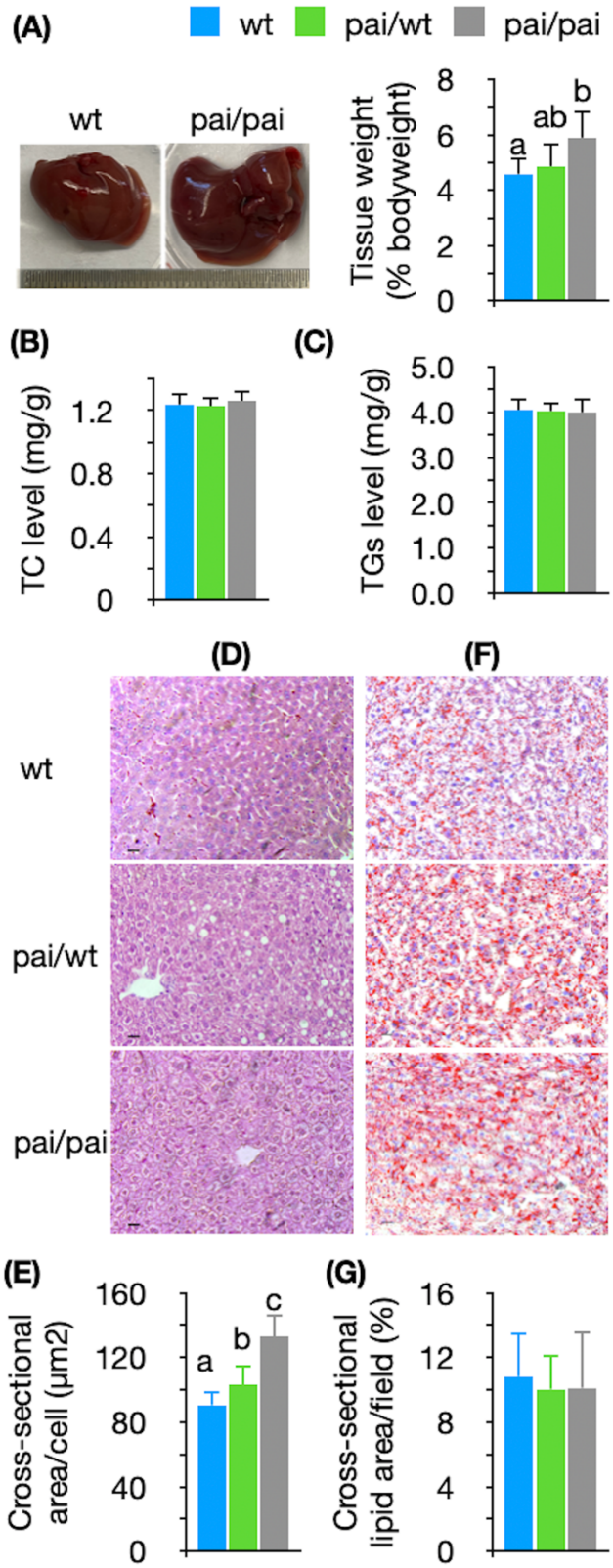

Figure 7. Lipid and histological analysis of livers. Comparison of weight (A), total cholesterol (B), and triglycerides (C) levels in wt and pai livers. Imaging of hematoxylin-eosin staining shows the abnormal morphology and oedema of pai hepatocytes. Analysis of cross-sectional area per cell indicates that the cellular volumes gradually enlarge in pai/wt and pai/pai hepatocytes, respectively (D-E, Bar = 10 μm). Oil red staining and analysis of the cross-sectional area of lipids per field show no lipid accumulation in either pai liver (G~H). Bars represent the mean ± SD, and different letters indicate $p < 0.05$.

Table 4. Relative expression of mRNAs in the livers

Genes	wt (n)	pai/pai (n)
Fatty acid and TGs synthesis		
Fatty acid synthase (*Fasn*)	1.03 ± 0.26 (14)	1.72 ± 0.56*** (13)
Stearoyl-CoA desaturase 1 (*Scd1*)	1.06 ± 0.41 (7)	1.19 ± 0.50 (5)
Fatty acid desaturase 1 (*Fads1*)	1.01 ± 0.21 (3)	1.08 ± 0.18 (3)
Fatty acid desaturase 2 (*Fads2*)	1.04 ± 0.33 (3)	0.92 ± 0.26 (3)
Peroxisome proliferator-activated receptor-γ (*Ppar-γ*)	1.04 ± 0.35 (28)	0.65 ± 0.31*** (23)
Glycerol-3-phosphate acyltransferase 1 (*Gpat1*)	1.05 ± 0.35 (7)	1.04 ± 0.37 (8)
1-acylglycerol-3-phosphate O-acyltransferase 2 (*Agpat2*)	1.02 ± 0.18 (15)	1.11 ± 0.25 (14)
Diacylglycerol acyltransferase-1 (*Dgat1*)	1.04 ± 0.28 (17)	1.37 ± 0.39* (15)
Diacylglycerol acyltransferase-2 (*Dgat2*)	1.03 ± 0.26 (9)	1.05 ± 0.32 (9)
CD36	1.07 ± 0.38 (8)	0.58 ± 0.32* (8)
Lipolysis and fatty acid oxidation		
Hepatic triglyceride lipase (*Htgl*)	1.06 ± 0.37 (9)	1.25 ± 0.28 (9)
Adipose triglyceride lipase (*Atgl*)	1.04 ± 0.33 (9)	1.03 ± 0.36 (9)
Hormone-sensitive lipase (*Hsl*)	1.07 ± 0.38 (9)	1.08 ± 0.26 (9)
Comparative gene identification 58 (*Cgi58*)	1.03 ± 0.27 (9)	1.40 ± 0.38* (9)
Lipoprotein lipase (*Lpl*)	0.99 ± 0.16 (11)	1.37 ± 0.15*** (6)
Carnitine palmitoyltransferase Ia (*Cpt1a*)	1.05 ± 0.37 (9)	1.01 ± 0.35 (9)
Long-chain acyl-CoA dehydrogenase (*Lcad*)	1.01 ± 0.18 (14)	1.11 ± 0.49 (14)
Medium-chain acyl-CoA dehydrogenase (*Mcad*)	1.06 ± 0.38 (15)	0.95 ± 0.36 (13)
Uncoupling protein 1 (*Ucp1*)	1.00 ± 0.31[a] (20)	0.59 ± 0.36** (13)
Uncoupling protein 2 (*Ucp2*)	1.04 ± 0.28 (16)	0.82 ± 0.28* (14)
Sterol pathway		
Liver X receptor α (*Lxrα*)	1.01 ± 0.16 (9)	1.15 ± 0.40 (9)
Liver X receptor β (*Lxrβ*)	1.02 ± 0.23 (9)	1.22 ± 0.47 (9)
Sterol Regulatory Element Binding Protein-1a (*Srebp1a*)	1.07 ± 0.39 (7)	1.54 ± 0.28* (7)
Sterol Regulatory Element Binding Protein-1c (*Srebp1c*)	1.12 ± 0.69 (4)	1.29 ± 0.44 (5)
Sterol Regulatory Element Binding Protein-2 (*Srebp2*)	1.00 ± 0.30 (16)	1.40 ± 0.71* (18)
HMG-CoA reductase (*Hmgcr*)	1.03 ± 0.27 (6)	0.65 ± 0.28* (7)
Insulin and IGF-1 signaling		
Insulin receptor (*Insr*)	0.99 ± 0.24 (16)	1.40 ± 0.34*** (17)
Insulin receptor substrate-1 (*Irs1*)	1.03 ± 0.28 (29)	1.19 ± 0.68 (25)
Insulin receptor substrate-2 (*Irs2*)	1.02 ± 0.34 (15)	1.55 ± 0.52** (16)

Table 4. Relative expression of mRNAs in the livers

Genes	wt (n)	pai/pai (n)
Insulin-like growth factor-1 (*Igf1*)	1.01 ± 0.23 (21)	1.40 ± 0.55** (22)
IGF binding protein 1 (*Igfbp1*)	1.01 ± 0.23 (15)	0.53 ± 0.26*** (18)
Forkhead box protein a2 (*Foxa2*)	1.03 ± 0.31 (27)	1.75 ± 0.77*** (30)
Igf1 receptor (*Igf1r*)	1.07 ± 0.37 (5)	1.63 ± 0.28* (4)
NADPH-producing		
Malic enzyme	1.02 ± 0.23 (8)	1.89 ± 0.93* (7)
Glucose-6-phosphate dehydrogenase (*G6pd*)	0.98 ± 0.19 (14)	2.34 ± 0.63*** (17)
6-Phosphogluconate dehydrogenase (*Pgd*)	1.24 ± 0.93 (8)	1.29 ± 0.80 (9)
Glucose metabolism and gluconeogenesis		
Glucose transporter type 4 (*Glut4*)	0.99 ± 0.23[a] (20)	0.59 ± 0.23*** (15)
Glucokinase	1.02 ± 0.23 (12)	0.66 ± 0.28** (13)
Carbohydrate response element binding protein (*Chrebp*)	1.00 ± 0.28 (13)	1.98 ± 0.60*** (11)
Fibroblast growth factor 21 (*Fgf21*)	1.32 ± 1.07 (9)	1.34 ± 0.91 (8)
Glucose-6-phosphatase (*G6p*)	1.02 ± 0.19 (14)	2.34 ± 0.63*** (25)
Phosphoenolpyruvate carboxykinase (*Pepck*)	1.06 ± 0.35 (13)	0.69 ± 0.31** (14)
Others		
AMP-activated protein kinase (*Ampk*)	1.06 ± 0.37 (9)	1.07 ± 0.35 (9)
Nuclear receptor subfamily 3 group C member 1 (*Nr3c1*)	1.03 ± 0.31 (3)	1.26 ± 0.36 (3)
F4/80	1.02 ± 0.20 (14)	1.45 ± 0.53* (13)
CD68	1.05 ± 0.34 (10)	0.76 ± 0.22* (10)
CD11c	1.05 ± 0.31 (19)	1.93 ± 0.89** (17)
Forkhead box protein c2 (*Foxc2*)	1.01 ± 0.17 (8)	1.59 ± 1.02 (10)
Pai	1.17 ± 0.69 (7)	10830 ± 8060* (7)

Numbers in brackets of the parameters indicate the size of tested samples. Each value represents the mean ± SD. * indicates $p < 0.05$; ** indicates $p < 0.01$; *** indicates $p < 0.001$, respectively.

387 genes ($p < 0.05$; Table 4), suggesting the t10c12-CLA might influence the liver metabolism in
388 mice.

389 Although the hepatic TC and TGs levels were normal in pai/pai mice, their hepatic
390 Srebp1a and Srebp2 were up-regulated, and the HMG-CoA reductase (Hmgcr) was down-
391 regulated. Some genes involved in FAs/TGs synthesis had also altered their transcription
392 levels. For instance, the RNA levels of Fasn, Dgat1 which convert diacylglycerol into TGs,
393 and Lpl which support FAs uptake, were increased; and the RNA levels of Ppar-γ and CD36,
394 which transport long-chain FAs into the cells, were decreased. Simultaneously, a series of
395 crucial enzymes involved in lipolysis and beta-oxidation kept standard transcription except for
396 the up-regulated Cgi58. In addition, the Ucp 1 and 2 engaged in thermogenesis were down-
397 regulated; the malic enzyme and G6pd, which both produce NADPH, were significantly up-
398 regulated; the inflammatory factors F4/80 and CD11c were up-regulated, but CD68 was down-
399 regulated (Table 4).

400 For genes involved in insulin/IGF1 signalling, except for reduced Igfbp1 and commonly
401 expressed Irs1, the other five essential genes, including Insr, Irs2, Igf1, Igf1 receptor, and
402 pioneering transcription factor Foxa2 were elevated together. For genes involved in glucose
403 metabolism and gluconeogenesis, the RNA levels of Glut4, glucokinase, and Pepck were
404 reduced, whereas the RNA levels of G6p and Chrebp were elevated. These transcriptional
405 changes suggest that t10c12-CLA easily influences hepatic glucose metabolism and insulin
406 sensitivity.

407 **3.9. Hypothalamic gene analysis**

408 To determine whether gene expression has been affected by t10c12-CLA in the
409 hypothalamus, which contains highly conserved neural circuitry controlling energy

Table 5. Relative expression of mRNAs in the hypothalamus

Genes	wt (n)	pai/wt (n)	pai/pai (n)
Insulin receptor (Insr)	1.01 ± 0.14[a] (8)	1.49 ± 0.64[ab] (4)	1.40 ± 0.34[b] (8)
Leptin receptor (Lepr)	1.02 ± 0.21[a] (9)	0.97 ± 0.39[a] (7)	1.60 ± 0.60[b] (8)
Ghrelin receptor (Ghsr)	1.03 ± 0.25[a] (8)	1.21 ± 0.43[a] (7)	1.80 ± 0.41[b] (6)
AMP-activated protein kinase (Ampk)	1.02 ± 0.20[a] (8)	1.41 ± 0.47[b] (9)	1.61 ± 0.51[b] (8)
Signal transducer and activator of transcription 3 (Stat3)	1.03 ± 0.27 (6)	1.11 ± 0.16 (7)	0.82 ± 0.45 (6)
Protein kinase B (Akt/PKB)	1.01 ± 0.14[a] (9)	1.84 ± 0.70[ab] (4)	1.63 ± 0.79[b] (10)
DEP domain containing MTOR-interacting protein (Deptor)	1.02 ± 0.24 (9)	1.49 ± 0.46 (4)	0.96 ± 0.28 (10)
Agouti-related peptide (Agrp)	1.03 ± 0.24[a] (14)	1.00 ± 0.33[a] (13)	1.88 ± 0.81[b] (11)
Neuropeptide Y (Npy)	1.02 ± 0.21[a] (14)	1.31 ± 0.35[b] (15)	1.74 ± 0.77[b] (11)
NPY postsynaptic receptor Y1 (Npy1r)	1.02 ± 0.22[a] (13)	1.44 ± 0.40[b] (8)	1.05 ± 0.35[a] (15)
Proopiomelanocortin (Pomc)	1.02 ± 0.21[a] (10)	1.31 ± 0.46[b] (14)	1.20 ± 0.31[ab] (8)
Cocaine- and amphetamine-regulated transcript (Cart)	1.00 ± 0.10[a] (7)	1.01 ± 0.07[a] (4)	0.80 ± 0.18[b] (8)
Melanocortic 4 receptor (Mc4r)	1.02 ± 0.24 (9)	1.16 ± 0.18 (4)	0.91 ± 0.20 (11)
glucose-regulated protein 78 (Grp78)	1.00 ± 0.03[a] (9)	1.31 ± 0.27[b] (7)	1.39 ± 0.31[b] (8)
Orexins	1.12 ± 0.40 (6)	0.96 ± 0.43 (7)	0.69 ± 0.63 (5)
Gonadtrophin releasing hormone (Gnrh)	1.03 ± 0.23[a] (12)	1.33 ± 0.24[b] (11)	1.44 ± 0.45[b] (13)
Arginine vasopressin (Avp)	1.02 ± 0.22[a] (8)	1.53 ± 0.34[b] (8)	2.15 ± 1.21[b] (8)
Corticotropin releasing hormone (Crh)	1.02 ± 0.22 (8)	1.05 ± 0.29 (10)	1.10 ± 0.37 (9)
Oxytocin	1.00 ± 0.10[a] (5)	1.47 ± 0.36[b] (7)	1.49 ± 0.40[b] (6)
Nuclear receptor subfamily 3 group C member 1 (Nr3c1)	1.03 ± 0.19[a] (7)	1.01 ± 0.26[a] (7)	1.93 ± 0.56[b] (6)
H19	1.02 ± 0.23 (9)	0.84 ± 0.23 (7)	0.82 ± 0.27 (7)
Ribonuclease type III (Dicer)	1.01 ± 0.15 (8)	0.86 ± 0.20 (7)	0.88 ± 0.21 (6)
DNA (cytosine-5)-methyltransferase 1 (Dnmt1)	1.00 ± 0.09[a] (6)		1.37 ± 0.32[b] (6)
Pai	1.05 ± 0.34[a] (8)	258 ± 137[b] (4)	356 ± 203[b] (6)

Numbers in brackets of the parameters indicate the size of tested samples. Each value represents the mean ± SD. Different letters in superscript indicate a level of statistical significance of $p < 0.05$.

410 metabolism, fluid and electrolyte balance, thermoregulation, responses to stressors, wake-sleep
411 cycles, and reproduction. The current study randomly chose 23 critical hypothalamic genes and
412 measured the transcriptional levels (Table 5).

413 Compared to wt samples, in the pai/pai hypothalamus, the RNA level changes were
414 observed in 14 (61%) genes. Only Cart, a marker of appetite-suppressive POMC neuron cells,
415 was down-regulated among them. The remaining 13 genes were up-regulated, including
416 appetite-relative genes such as the Insulin receptor, ghrelin receptor, agouti-related peptide,
417 neuropeptide Y, leptin receptor, and the intracellularly signal molecule Akt/PKB, suggesting
418 the sensitivity in regulating energy balance. In addition, the up-regulated gonadotrophin-
419 releasing hormone, oxytocin, arginine vasopressin, DNA methyltransferase-1, and Nr3c1,
420 suggesting that t10c12-CLA might affect the various neural circuitry in the hypothalamus.
421 Furthermore, the RNA levels of Ampk and molecular chaperone Grp78 which releases the
422 endoplasmic reticulum pressure and transmits thermogenesis signals to the BAT tissues were
423 increased in the pai/pai hypothalamus. However, western blot analysis revealed that the protein
424 levels of AMPK, pAMPK and GRP78 were not altered in the pai/pai hypothalamus compared
425 with the wt samples (Fig. 8 A-B).

426 In the pai/wt hypothalamus, the RNA levels of eight (36%) genes, including Ampk, Npy,
427 Npy postsynaptic receptor Y1, Pomc, Grp78, GnRH, oxytocin, and arginine vasopressin, were
428 increased, and no tested genes were down-regulated in pai/wt hypothalamus. Between pai/wt
429 and pai/pai samples, the RNA levels of six (27%) genes, including Lepr, Ghsr, Agrp, Npy
430 postsynaptic receptor Y1, Cart, and Nr3c1 exhibited differences ($p < 0.05$), suggesting the
431 genotype-specific transcription in the hypothalamus.

432

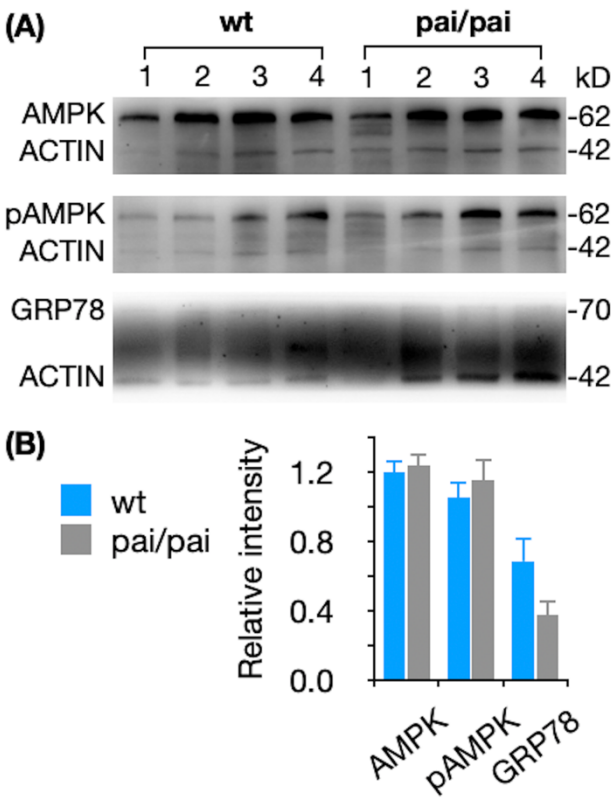

Figure 8. Western blot images (A) and relative intensities (B) analyses of some critical proteins in the hypothalamus from wt and pai/pai mice. ACTIN, beta-actin; GRP78, glucose-regulated protein 78; (p)AMPK, (phosphorylated) AMP-activated protein kinase. Bars represent the mean ± SD.

433 **4. Discussion**

434 Unlike the temporary fat loss in the body [24] or milk fat depression which the fat de
435 novo synthesis would reverse after the termination of the t10c12-CLA supplementation in mice
436 [8], in pai mice, the chronic t10c12-CLA resulted in an irreversible fat reduction. It may cause
437 an adaptive metabolic response throughout the entire developmental stage. Metabolic
438 compensation or adaptation to t10c12-CLA is intrinsically complicated owing to its diverse
439 metabolic functions in multiple target organs. Thus, the interpretation of these data could be
440 more explicit in pai mice.

441 Although the fat reduction in milk did not impact the body weight of piglets from the
442 energy supply perspective [25], previous studies in mice indicated that the dietary t10c12-CLA
443 could reduce milk fat and retard pup growth [8, 26]. However, we found that the wt pups
444 fostered by the pai mother were reversely overweight at three weeks, suggesting that the natural
445 t10c12-CLA from the mothers might play an active role during offspring development and
446 more work needs to be done in future.

447 When a mouse was fed a low-fat diet containing t10c12-producing lactic acid bacteria or
448 0.4~1% t10c12-CLA, its fat loss happened quickly, as early as seven days after starting the
449 t10c12-CLA diet [13, 24, 27] and the body fat could reduce from approximately 2.8 g to less
450 than 0.4 g in C57BL/6J males [28]. Simultaneously, the contents of t10c12-CLA were 0.1% in
451 the livers of Balb/c males [7], approximately 0.2% in various tissues of ICR females [9], 0.45%
452 in the milk of C57BL/6J females [8], 0.013 μmol/g in the brain or 0.089 μmol/g t10c12-CLA
453 in eye lipids of C57BL/6N females [12]. Similarly, in the current study, the comparable values
454 of t10c12-CLA were also detected in transgenic hearts (8.85 μg/g, 0.09%), livers (16.65 μg/g,

455 0.19%), kidneys (11.33 μg/g, 0.09%), BAT (28.8 μg/g, 0.23%), or WAT (4.89 μg/g, 0.13%;
456 Supplemental Table 4) in pai mice.

457 Studies on whether the dietary t10c12-CLA plays a role in food intake or appetite showed
458 contradictory results in mice [4, 6, 27, 29]. In pai mice, we had not observed any changes in
459 food intake within metabolic cages or crucial circulating leptin, insulin, glucose, and ghrelin.
460 The results suggest that the anti-obesity property of t10c12-CLA is independent of food intake
461 or appetite. On the other hand, the hypothalamic RNA increases in receptors for insulin, leptin,
462 and ghrelin, and vital appetite-relative genes Npy, Argp, and an RNA decrease in appetite-
463 suppressive Cart imply a tendency to promote food intake, which the feedback regulation
464 mechanism might cause after more heat release, for the hormonal receptors, neuropeptides and
465 energy sensor AMPK is in a complex regulation and interplay of energy homeostasis in the
466 hypothalamic cells.

467 Studies of oral t10c12-CLA administration suggested that the fat loss mainly occurred in
468 fat depots through modulating adipocyte metabolism, such as increased fatty acid oxidation
469 and browning WAT [2, 13, 30], or increasing the number of beige adipocytes in mice [28]. The
470 pai/pai mice here reduced the WAT mass by approximately 20% at 11 weeks. However, RNA
471 analysis indicated reduced pai/pai WAT browning and gluconeogenesis. Interestingly, the
472 beta-oxidation of very long-chain FAs in peroxisomes was increased. That was, the pai/pai
473 mice had adapted to long-term t10c12-induced fat reduction and could decrease the browning
474 of WAT and mobilise the energy from the very long-chain FAs to maintain energy
475 homeostasis.

476 Studies on whether the dietary t10c12-CLA modulates hepatic lipid metabolism and even
477 induces fatty liver also showed contradictory results in mice [5, 13, 24, 31, 32]. It was supposed

478 that the t10c12-induced hepatic steatosis might be due to the uptake and accumulation of lipids
479 mobilised from the adipose tissue [5]. In the current study, although the essential genes Fasn,
480 Dgat1, and Lpl involved in TGs uptake and synthesis were up-regulated in hepatocytes,
481 analysis of hepatic TGs and TC levels and slices indicated no steatosis in pai livers.
482 Furthermore, the blood TGs concentration was also lowered in pai mice, similar to the reduced
483 plasma TGs in mice treated with a high dose of t10c12-CLA (0.6% w/w) [33]. A study in
484 lactating mice suggested that dietary t10c12-CLA might not induce fat accumulation in the
485 liver when plenty of energy was consumed for lactation [8]. In pai mice, more energy
486 expenditure via increased thermogenesis also hinted that no surplus energy could be
487 accumulated in the liver. Our results suggest that the t10c12-CLA has yet to break local lipid
488 homeostasis in the livers thoroughly.

489 A study in female 129Sv/J retired breeders indicated that dietary CLA mixture could
490 induce body fat reduction via increasing energy expenditure [4]. Unfortunately, this work has
491 yet to clarify whether the energy expenditure is via exercise strengthening or fat burning. Here,
492 increased heat release accompanied by reduced activities in pai/pai mice suggests that body fat
493 reduction results from increased thermogenesis. Additionally, the levels of circulating PGE2,
494 adrenaline, corticosterone, TNF-α, Il-6, and CRP in pai mice also suggest that the increased
495 heat production is not due to the response to bacterial PAI enzyme-induced stress and/or
496 inflammation in pai mice.

497 BAT thermogenesis can account for up to 50% of the body's energetic maintenance
498 demand. An increase [9] or decrease in BAT mass [33] were respectively observed in t10c12-
499 CLA treated mice, but in pai/pai mice, the increased BAT mass might correlate with more heat
500 release; additionally, the over-expression of pAMPK that phosphorylates key targets to rewire
501 a variety of metabolic processes and UCP2 proteins in the pai/pai brown adipocytes also

502 suggest increased thermogenesis via BAT activation. Based on the phenotypic characteristics
503 of pai mice, the authors suspected that the excess FGF21 in the blood and the central regulatory
504 mechanism might be involved in the t10c12-CLA-induced BAT thermogenesis.

505 FGF21 functions as a master sensitiser of specific hormonal signalling involved in
506 enhancing insulin sensitivity and lowering serum glucose through direct actions on adipose
507 tissues, possibly through the FGF21/adiponectin/ceramide axis [34], increasing energy
508 expenditure through immediate efforts on the central nervous system to stimulate BAT
509 thermogenesis, decreasing hepatic oxidative stress [35], lowering plasma TGs by accelerating
510 lipoprotein catabolism in WAT and BAT [36], and regulating macronutrient preference [23].
511 In the current study, excess FGF21 in the blood and local FGF21 expression in the BAT tissues
512 suggest that the circulating FGF21 plays an active role in BAT thermogenesis. Additionally,
513 the observable characteristics in pai/wt mice, such as an increase in FAs content in the kidney,
514 body weight increase during adulthood, blood glucose sensitivity, serum TGs decrease, and
515 genotype-specific gene expression in various tissues would be associated with the excess
516 FGF21. We have yet to pay more attention to unique features in pai/wt mice here, and further
517 work needs to be done in the future.

518 AMPK in the ventromedial nucleus of the hypothalamus can decrease ceramide-induced
519 endoplasmic reticulum (ER) stress which stimulates the thermogenic program in BAT through
520 the sympathetic nervous system [37]. In addition, GRP78 over-expression in the ventromedial
521 nucleus can ameliorate hypothalamic ER stress, leading to weight loss, reduced hepatic
522 steatosis, improved insulin and leptin sensitivities, increased BAT thermogenesis and
523 stimulation WAT browning [38, 39]. In the pai hypothalamus, the up-regulated transcriptional
524 levels of Ampk and Grp78 suggest that the hypothalamic neurons might promote heat

525 production via ameliorating ER stress in pai/pai mice. Unfortunately, we had not observed
526 evident changes in the hypothalamic AMPK, pAMPK and GRP78 proteins.

527 Focused on increased thermogenesis, more work needs to clarify if the t10c12-CLA
528 might affect ceramide in various ways: 1) the sphingomyelinase pathway to break down
529 sphingomyelin in the plasma membrane to release ceramide; 2) de novo synthesis of ceramide
530 from the condensation of palmitic acid (16:0) and serine to form 3-keto-dihydrosphingosine in
531 the ER; or 3) the salvage pathway to break down sphingolipids to sphingosine in the lysosomes
532 and to form ceramide by re-acylation in the ventromedial nucleus.

533 In addition, the expression modification of other hypothalamic genes, such as GCs
534 receptor Nr3c1, required negative regulation of the hypothalamic–pituitary–adrenal axis at a
535 basal condition and under stress [40]; vasopressin involved in fluid and electrolyte balance;
536 GnRH and oxytocin involved in reproduction; even imprinted H19 and Dnmt1 involved in the
537 epigenetic modification, were also observed in the pai hypothalamus. These aberrant
538 expressions of hypothalamic genes suggest that the t10c12-CLA might play active roles in the
539 myriad neural circuits in the hypothalamus and a more complex mechanism of action of
540 t10c12-CLA needs to be investigated further.

Acknowledgement

We thank Dr Li-Li Song and graduate students Yun-Cheng Zhuang, Yu-Huang Chen, Chao Wang, Qi Wang, Mei Liu, and Jia-Qi Lu in our lab for their generous assistance in partial tests and Ms Yu-Yang Wang in our university for technique help in gas chromatography. We also thank Professor Hong-Jun Wang at the Medical University of South Carolina, USA, for the helpful discussion during the writing process and Ms Wen-Jing Gou's language help in preparing this manuscript.

Funding sources

This work was supported by the National Key Research and Development Program of China (2018YFC1003800) and a Project Funded by the Priority Academic Program Development of Jiangsu Higher Education Institutions (PAPD). The Jiangsu Funding Program for Excellent Postdoctoral Talent supported Rao Y.

CRediT Authorship Contributions

Yu Rao: Conceptualization; Data curation; Formal analysis; Funding acquisition; Investigation; Methodology; Software; Roles/Writing - original draft. Shi-Li Li: Conceptualization; Formal analysis. Mei-Juan Li, Bao-Zhu Wang, Yang-Yang Wang, Lu-Wen Liang: Data curation; Investigation; Methodology. Shuai Yu, Zong-Ping Liu: Data curation; Software; Validation; Visualization. Sheng Cui: Conceptualization; Funding acquisition; Project administration. Ke-Mian Gou: Conceptualization; Formal analysis; Funding acquisition; Project administration; Supervision; Writing - review & editing.

All authors proofread, made comments, and approved the report.

Competing Interest Statement

The authors declare no competing interests.

Data access

The data supporting the findings of this study are available from the corresponding author upon reasonable request.

Supplementary data

This manuscript contains supplementary data.

References

[1] Ritzenthaler KL, McGuire MK, McGuire MA, Shultz TD, Koepp AE, Luedecke LO, et al. Consumption of conjugated linoleic acid (CLA) from CLA-enriched cheese does not alter milk fat or immunity in lactating women. J Nutr 2005;135:422-30. http://doi.org/10.1093/jn/135.3.422.

[2] Park Y, Albright KJ, Liu W, Storkson JM, Cook ME, Pariza MW. Effect of conjugated linoleic acid on body composition in mice. Lipids 1997;32:853-8. http://doi.org/10.1007/s11745-997-0109-x.

[3] Baumgard LH, Corl BA, Dwyer DA, Saebo A, Bauman DE. Identification of the conjugated linoleic acid isomer that inhibits milk fat synthesis. Am J Physiol Regul Integr Comp Physiol 2000;278:R179-84. http://doi.org/10.1152/ajpregu.2000.278.1.R179.

[4] Park Y, Park Y. Conjugated nonadecadienoic acid is more potent than conjugated linoleic acid on body fat reduction. J Nutr Biochem 2010;21:764-73. http://doi.org/10.1016/j.jnutbio.2009.05.003.

[5] Vyas D, Kadegowda AK, Erdman RA. Dietary conjugated linoleic Acid and hepatic steatosis: species-specific effects on liver and adipose lipid metabolism and gene expression. J Nutr Metab 2012;2012:932928. http://doi.org/10.1155/2012/932928.

[6] Kim JH, Kim Y, Kim YJ, Park Y. Conjugated Linoleic Acid: Potential Health Benefits as a Functional Food Ingredient. Annu Rev Food Sci Technol 2016;7:221-44. http://doi.org/10.1146/annurev-food-041715-033028.

[7] Rosberg-Cody E, Stanton C, O'Mahony L, Wall R, Shanahan F, Quigley EM, et al. Recombinant lactobacilli expressing linoleic acid isomerase can modulate the fatty acid composition of host adipose tissue in mice. Microbiol-Sgm 2011;157:609-15. http://doi.org/10.1099/mic.0.043406-0.

[8] Harvatine KJ, Robblee MM, Thorn SR, Boisclair YR, Bauman DE. Trans-10, cis-12 CLA dose-dependently inhibits milk fat synthesis without disruption of lactation in C57BL/6J mice. J Nutr 2014;144:1928-34. http://doi.org/10.3945/jn.114.198911.

[9] Li SL, Ma SY, Xu BR, Fan ZY, Li MJ, Cao WG, et al. Effects of trans-10, cis-12-conjugated linoleic acid on mice are influenced by the dietary fat content and the degree of murine obesity. Eur J Lipid Sci Tech 2015;117:1908-18. http://doi.org/10.1002/ejlt.201400568.

[10] Adkins Y, Belda BJ, Pedersen TL, Fedor DM, Mackey BE, Newman JW, et al. Dietary Docosahexaenoic Acid and trans-10, cis-12-Conjugated Linoleic Acid Differentially Alter Oxylipin Profiles in Mouse Periuterine Adipose Tissue. Lipids 2017;52:399-413. http://doi.org/10.1007/s11745-017-4252-3.

[11] So MH, Tse IM, Li ET. Dietary fat concentration influences the effects of trans-10, cis-12 conjugated linoleic acid on temporal patterns of energy intake and hypothalamic expression

of appetite-controlling genes in mice. J Nutr 2009;139:145-51. http://doi.org/10.3945/jn.108.093849.

[12] Vemuri M, Adkins Y, Mackey BE, Kelley DS. Docosahexaenoic Acid and Eicosapentaenoic Acid Did not Alter trans-10,cis-12 Conjugated Linoleic Acid Incorporation into Mice Brain and Eye Lipids. Lipids 2017;52:763-9. http://doi.org/10.1007/s11745-017-4282-x.

[13] Shen W, Baldwin J, Collins B, Hixson L, Lee KT, Herberg T, et al. Low level of trans-10, cis-12 conjugated linoleic acid decreases adiposity and increases browning independent of inflammatory signaling in overweight Sv129 mice. J Nutr Biochem 2015;26:616-25. http://doi.org/10.1016/j.jnutbio.2014.12.016.

[14] Marques TM, Wall R, O'Sullivan O, Fitzgerald GF, Shanahan F, Quigley EM, et al. Dietary trans-10, cis-12-conjugated linoleic acid alters fatty acid metabolism and microbiota composition in mice. Br J Nutr 2015;113:728-38. http://doi.org/10.1017/S0007114514004206.

[15] Oteng AB, Kersten S. Mechanisms of action of trans fatty acids. Adv Nutr 2020;11:697-708. http://doi.org/10.1093/advances/nmz125.

[16] Kohno-Murase J, Iwabuchi M, Endo-Kasahara S, Sugita K, Ebinuma H, Imamura J. Production of trans-10, cis-12 conjugated linoleic acid in rice. Transgenic Res 2006;15:95-100. http://doi.org/10.1007/s11248-005-3736-8.

[17] Wang C, Wang YY, Rao Y, Li MJ, Liu ZP, Li SL, et al. Heterologous expression of Propionibacterium acnes isomerase in mouse (Mus musculus) cells and production of t10c12-conjugated linoleic acid. Chinese Journal of Agricultural Biotechnology 2021;29:2304-11. http://doi.org/10.3969/j.issn.1674-7968.2021.12.004.

[18] Li SL. Analysis of the effect of trans 10, cis 12-conjugated linoleic acid on mice growth and metabolism. Ph.D. Dissertation. Beijing: China Agricultural University; 2015.

[19] Li M, Li S, Rao Y, Cui S, Gou K. Loss of smooth muscle myosin heavy chain results in the bladder and stomach developing lesion during foetal development in mice. J Genet 2018;97:469-75.

[20] Chu VT, Weber T, Graf R, Sommermann T, Petsch K, Sack U, et al. Efficient generation of Rosa26 knock-in mice using CRISPR/Cas9 in C57BL/6 zygotes. BMC Biotechnol 2016;16:4. http://doi.org/10.1186/s12896-016-0234-4.

[21] Jenkins TC. Technical note: common analytical errors yielding inaccurate results during analysis of fatty acids in feed and digesta samples. J Dairy Sci 2010;93:1170-4. http://doi.org/10.3168/jds.2009-2509.

[22] Chen HC, Farese RV, Jr. Determination of adipocyte size by computer image analysis. J Lipid Res 2002;43:986-9.

[23] Flippo KH, Potthoff MJ. Metabolic Messengers: FGF21. Nat Metab 2021;3:309-17. http://doi.org/10.1038/s42255-021-00354-2.

[24] Cordoba-Chacon J, Sugasini D, Yalagala PCR, Tummala A, White ZC, Nagao T, et al. Tissue-dependent effects of cis-9,trans-11- and trans-10,cis-12-CLA isomers on glucose and lipid metabolism in adult male mice. J Nutr Biochem 2019;67:90-100. http://doi.org/10.1016/j.jnutbio.2019.01.020.

[25] Sandri EC, Harvatine KJ, Oliveira DE. Trans-10, cis-12 conjugated linoleic acid reduces milk fat content and lipogenic gene expression in the mammary gland of sows without altering litter performance. Br J Nutr 2020;123:610-8. http://doi.org/10.1017/S0007114519003325.

[26] Robblee MM, Boisclair YR, Bauman DE, Harvatine KJ. Dietary Fat Does Not Overcome trans-10, cis-12 Conjugated Linoleic Acid Inhibition of Milk Fat Synthesis in Lactating mice. Lipids 2020;55:201-12. http://doi.org/10.1002/lipd.12228.

[27] Shelton VJ, Shelton AG, Azain MJ, Hargrave-Barnes KM. Incorporation of conjugated linoleic acid into brain lipids is not necessary for conjugated linoleic acid-induced reductions in feed intake or body fat in mice. Nutr Res 2012;32:827-36. http://doi.org/10.1016/j.nutres.2012.10.003.

[28] Yeganeh A, Zahradka P, Taylor CG. Trans-10,cis-12 conjugated linoleic acid (t10-c12 CLA) treatment and caloric restriction differentially affect adipocyte cell turnover in obese and lean mice. Journal of Nutritional Biochemistry 2017;49:123-32. http://doi.org/10.1016/j.jnutbio.2017.08.003.

[29] Park Y, Albright KJ, Storkson JM, Liu W, Pariza MW. Conjugated linoleic acid (CLA) prevents body fat accumulation and weight gain in an animal model. J Food Sci 2007;72:S612-7. http://doi.org/10.1111/j.1750-3841.2007.00477.x.

[30] den Hartigh LJ, Wang SR, Goodspeed L, Wietecha T, Houston B, Omer M, et al. Metabolically distinct weight loss by 10,12 CLA and caloric restriction highlight the importance of subcutaneous white adipose tissue for glucose homeostasis in mice. Plos One 2017;12. http://doi.org/ARTN e0172912

10.1371/journal.pone.0172912.

[31] Ashwell MS, Ceddia RP, House RL, Cassady JP, Eisen EJ, Eling TE, et al. Trans-10, cis-12-conjugated linoleic acid alters hepatic gene expression in a polygenic obese line of mice displaying hepatic lipidosis. J Nutr Biochem 2010;21:848-55. http://doi.org/10.1016/j.jnutbio.2009.06.013.

[32] Kostogrys RB, Franczyk-Zarow M, Maslak E, Gajda M, Mateuszuk L, Chlopicki S. Effects of margarine supplemented with t10c12 and C9T11 CLA on atherosclerosis and steatosis in apoE/LDLR -/- mice. J Nutr Health Aging 2012;16:482-90. http://doi.org/10.1007/s12603-011-0354-4.

[33] Shen W, Chuang CC, Martinez K, Reid T, Brown JM, Xi L, et al. Conjugated linoleic acid reduces adiposity and increases markers of browning and inflammation in white adipose tissue of mice. J Lipid Res 2013;54:909-22. http://doi.org/10.1194/jlr.M030924.

[34] Holland WL, Adams AC, Brozinick JT, Bui HH, Miyauchi Y, Kusminski CM, et al. An FGF21-adiponectin-ceramide axis controls energy expenditure and insulin action in mice. Cell Metab 2013;17:790-7. http://doi.org/10.1016/j.cmet.2013.03.019.

[35] Ye D, Wang Y, Li H, Jia W, Man K, Lo CM, et al. Fibroblast growth factor 21 protects against acetaminophen-induced hepatotoxicity by potentiating peroxisome proliferator-activated receptor coactivator protein-1alpha-mediated antioxidant capacity in mice. Hepatology 2014;60:977-89. http://doi.org/10.1002/hep.27060.

[36] Schlein C, Talukdar S, Heine M, Fischer AW, Krott LM, Nilsson SK, et al. FGF21 Lowers Plasma Triglycerides by Accelerating Lipoprotein Catabolism in White and Brown Adipose Tissues. Cell Metab 2016;23:441-53. http://doi.org/10.1016/j.cmet.2016.01.006.

[37] Martinez-Sanchez N, Seoane-Collazo P, Contreras C, Varela L, Villarroya J, Rial-Pensado E, et al. Hypothalamic AMPK-ER Stress-JNK1 Axis Mediates the Central Actions of Thyroid Hormones on Energy Balance. Cell Metab 2017;26:212-29 e12. http://doi.org/10.1016/j.cmet.2017.06.014.

[38] Contreras C, Gonzalez-Garcia I, Seoane-Collazo P, Martinez-Sanchez N, Linares-Pose L, Rial-Pensado E, et al. Reduction of Hypothalamic Endoplasmic Reticulum Stress Activates Browning of White Fat and Ameliorates Obesity. Diabetes 2017;66:87-99. http://doi.org/10.2337/db15-1547.

[39] Contreras C, Fondevila MF, Lopez M. Hypothalamic GRP78, a new target against obesity? Adipocyte 2018;7:63-6. http://doi.org/10.1080/21623945.2017.1405878.

[40] Laryea G, Schutz G, Muglia LJ. Disrupting hypothalamic glucocorticoid receptors causes HPA axis hyperactivity and excess adiposity. Mol Endocrinol 2013;27:1655-65. http://doi.org/10.1210/me.2013-1187.